Geoscience Frontiers 11 (2020) 2347–2364

HOSTED BY

Contents lists available at ScienceDirect

Geoscience Frontiers

journal homepage: www.elsevier.com/locate/gsf

Research Paper

Petrology and geochemistry of mafic and ultramafic cumulate rocks from the eastern part of the Sabzevar ophiolite (NE Iran): Implications for their petrogenesis and tectonic setting

Fatemeh Rahmani [a], Mohamad Ali Mackizadeh [a,*], Moussa Noghreyan [a], Claudio Marchesi [b,c], Carlos J. Garrido [b]

[a] Department of Geology, Faculty of Sciences, University of Isfahan, P.O. Box: 81746-73441, Isfahan, Iran
[b] Instituto Andaluz de Ciencias de La Tierra (IACT), CSIC-Universidad de Granada, Avenida de Las Palmeras 4, 18100, Armilla, Granada, Spain
[c] Departamento de Mineralogía y Petrología, Facultad de Ciencias, Universidad de Granada, Avenida Fuentenueva s/n, 18002, Granada, Spain

ARTICLE INFO

Handling Editor: Kristoffer Szilas

Keywords:
Petrology
Geochemistry
Cumulate rocks
Sabzevar ophiolite
Supra-subduction zone
Iran

ABSTRACT

The Late Cretaceous Sabzevar ophiolite represents one of the largest and most complete fragments of Tethyan oceanic lithosphere in the NE Iran. It is mainly composed of serpentinized mantle peridotites slices; nonetheless, minor tectonic slices of all crustal sequence constituents are observed in this ophiolite. The crustal sequence contains a well-developed ultramafic and mafic cumulates section, comprising plagioclase-bearing wehrlite, olivine clinopyroxenite, olivine gabbronorite, gabbronorite, amphibole gabbronorite and quartz gabbronorite with adcumulate, mesocumulate, heteradcumulate and orthocumulate textures. The crystallization order for these rocks is olivine ± chromian spinel → clinopyroxene → plagioclase → orthopyroxene → amphibole. The presence of primary magmatic amphiboles in the cumulate rocks shows that the parent magma evolved under hydrous conditions. Geochemically, the studied rock units are characterized by low TiO_2 (0.18–0.57 wt.%), P_2O_5 (<0.05 wt.%), K_2O (0.01–0.51 wt.%) and total alkali contents (0.12–3.04 wt.%). They indicate fractionated trends in the chondrite-normalized rare earth element (REE) plots and multi-element diagrams (spider diagrams). The general trend of the spider diagrams exhibit slight enrichment in large ion lithophile elements (LILEs) relative to high field strength elements (HFSEs) and positive anomalies in Sr, Pb and Eu and negative anomalies in Zr and Nb relative to the adjacent elements. The REE plots of these rocks display increasing trend from La to Sm, positive Eu anomaly (Eu/Eu* = 1.06–1.54) and an almost flat pattern from medium REE (MREE) to heavy REE (HREE) region [$(Gd/Yb)_N$ = 1–1.17]. Moreover, clinopyroxenes from the cumulate rocks have low REE contents and show marked depletion in light REE (LREE) compared to MREE and HREE [$(La/Sm)_N$ = 0.10–0.27 and $(La/Yb)_N$ = 0.08–0.22]. The composition of calculated melts in equilibrium with the clinopyroxenes from less evolved cumulate samples are closely similar to island arc tholeiitic (IAT) magmas. Modal mineralogy, geochemical features and REE modeling indicate that Sabzevar cumulate rocks were formed by crystal accumulation from a hydrous depleted basaltic melt with IAT affinity. This melt has been produced by moderate to high degree (~15%) of partial melting a depleted mantle source, which partially underwent metasomatic enrichment from subducted slab components in an intra-oceanic arc setting.

1. Introduction

Ultramafic and mafic cumulate rocks are obvious evidence of the presence of magma chambers and give information about the depth, thermal history and size of magma reservoirs, as well as help to constrain models of basalt differentiation. They are formed by the injection of basaltic melt from the underlying rising mantle and are regarded as created by slow crystallization in a magma chamber (Gass, 1989). These rocks are found in different tectonic environments, such as oceanic lower crust generated at spreading ocean ridges, ophiolites in the active orogenic regions, Alaskan-type complexes in the subduction-related environments and large stratiform complexes in non-orogenic domains

* Corresponding author.
E-mail address: mackizadeh55@gmail.com (M.A. Mackizadeh).
Peer-review under responsibility of China University of Geosciences (Beijing).

https://doi.org/10.1016/j.gsf.2020.02.004
Received 25 June 2019; Received in revised form 21 December 2019; Accepted 8 February 2020
Available online 27 February 2020

(Deng et al., 2015; Pál-Molnár et al., 2015, and references therein). Different petrological and geochemical features of ultramafic and mafic cumulate sequences can be used to identify the tectonic environment, constrain the nature of mantle source and provide new insights into the processes controlling the formation and evolution of mantle-derived melts (Meyer et al., 1989; Wilson, 1989; Greene et al., 2006; Jagoutz et al., 2006; Tribuzio et al., 2008; Piccardo and Guarnieri, 2011, and references therein; Gahlan et al., 2012; Allahyari et al., 2014; Deng et al., 2015; Pál-Molnár et al., 2015; Tanirli and Rizaoglu, 2016; Camuzcuoğlu et al., 2017; Dey et al., 2018).

Ophiolites are considered as sections of ancient oceanic lithosphere that have been tectonically located along continental margins during tectonic events such as collision and obduction (Coleman, 1977; Dilek, 2003; Dilek and Furnes, 2011, 2014; Saccani et al., 2015). They have been generated in a wide variety of geotectonic settings, of which mid-oceanic spreading ridges (MOR) and SSZ environments including intra-oceanic arcs, continental arcs, fore-arcs and back-arcs are the major ones (Sun and Nesbitt, 1978; Beccaluva et al., 1979; Saunders et al., 1980; Serri, 1981; Shervais, 2001; Pearce, 2003, 2008; Stern, 2004; Metcalf and Shervais, 2008; Dilek and Furnes, 2011; Saccani et al., 2011; Saccani, 2015). Ophiolites are important sources of information for understanding processes acting at mid-ocean ridges, marginal basins and subduction zone settings, as well as distinguishing rock types that form oceanic lithosphere. Geochemistry of ophiolitic rocks is generally applied to identify their tectonic settings and composition of parental magmas and mantle sources.

The Sabzevar ophiolite is one of several remnants of Neotethyan oceanic lithosphere in the northeast of Iran (Fig. 1a). This ophiolite is tectonically dismembered but all the elements of a complete ophiolite are present. Petrological studies on the different parts of the Sabzevar ophiolite indicated formation in a SSZ setting and a IAT affinity for the Sabzevar sheeted dikes, and N-MORB (normal mid–ocean ridge basalt), E-MORB (enriched MORB), IAT and calc-alkaline to almost alkaline affinities for extrusive rocks of the Sabzevar ophiolite (Noghreyan, 1982; Shojaat et al., 2003; Khalatbari Jafari et al., 2013a, b; Shafaii Moghadam et al., 2013, 2014; Rahmani et al., 2017; Rahmani, 2018; Rezaei et al., 2018).

The Sabzevar ophiolite has a well-developed ultramafic and mafic cumulate sequence. Cumulate rocks form a part of crustal section in some of ophiolitic sequences. They are formed by slow crystallization mantle-derived melts in magma chambers. Their geochemical and petrological characters provide significant information about origin and tectonic evolution of oceanic lithosphere and record the history of melt transport and crystallization between mantle and seafloor (Pearce, 2008; Saccani, 2015). A previous study on the mineral chemistry of cumulate rocks from the Sabzevar ophiolite indicated that they were formed in an arc-related/SSZ setting as a consequence of high- to low-pressure crystallization from a basaltic melt in an active magma chamber situated at the base of the crust (Rahmani et al., 2017). In this study, we present new geochemical data from whole rock and clinopyroxenes of the cumulate rocks from the Sabzevar ophiolite to (1) provide a detailed study of their geochemical characteristics of them, (2) show geochemical similarities between the studied rock units and equivalents from different tectonic settings and other ophiolites, (3) determine their original tectonic setting and parental magma composition and (4) characterize the composition and partial melting conditions of the mantle source.

2. Geological setting

Iranian ophiolites are part of the Middle East Tethyan ophiolites (Hassanipak and Ghazi, 1999), which have been tectonically emplaced into the thrust mountain belts of Iran. Based on their age and geographical location, they have been classified into five groups (Fig. 1a) (Torabi et al., 2011, 2013; Shafaii Moghadam and Stern, 2015): (1) Paleozoic metaophiolites that emplaced in the western part of the Central-East Iranian Microcontinent (CEIM), including the Anarak, Jandaq, Posht–e–Badam and Bayazeh ophiolites; (2) Paleozoic ophiolites of northern Iran, which consists of the Aghdarband, Mashhad, Takab and Rasht ophiolites; (3) Mesozoic ophiolites located along the Zagros thrust zone including the Neyriz and Kermanshah ophiolites, which are regarded as the extension of the Oman ophiolites that was emplaced onto the Arabian continental margin; (4) Mesozoic ophiolites of the Makran accretionary prism, including the Band-e-Zeyarat, Dar Anar, and Fanuj-Maskutan complexes and (5) Mesozoic ophiolites and ophiolitic mélanges at the periphery of the CEIM including the Nain, Baft, Sabzevar, Tchehel–Kureh and Birjand ophiolites. The Paleozoic ophiolites are considered to be the Palaeotethys suture zones, while the Mesozoic ophiolites represent the Neotethys suture zones. The main Neotethys suture zone is placed along the Zagros Mountain range and is traceable westward into Turkey, where it connects to the Izmir-Ankara suture zone (Omrani et al., 2013, and references therein).

The ophiolites peripheral to the CEIM are considered as remnants of oceanic basins related to the Neotethys including: (1) the Sistan Ocean, in eastern Iran, that separated the CEIM from the Farah and Helmand blocks, (2) the Fanuj Ocean, in the south and southwest of Iran, between the CEIM and the Sanadaj-Sirjan/Afro-Arabian plate and (3) the Sabzevar Ocean, in northern Iran, that separated the CEIM from the Kopeh-Dagh zone (Turan plate) (Takin, 1972; Stöcklin, 1974; Berberian and King, 1981; Sengör, 1990; Arvin and Robinson, 1994; Shojaat et al., 2003). However, Rossetti et al. (2010) suggested that the Late Cretaceous Sabzevar and Nain ophiolites were parts of the same unit and formed in a back-arc basin associated with the subduction of the Sistan Ocean. Moreover, recent studies base on the paleomagnetic and paleogeography of Central Iran and chemical features of volcanic rocks from different ophiolites around the CEIM (Mattei et al., 2012, 2014; Pirnia et al., 2020) proposed that Sabzevar and Nain ophiolites formed in the northwestern prolongation sector of the Sistan Ocean.

The Sabzevar ophiolite is a dismembered ophiolitic complex, which covers an area over 3000 km^2 from 56°12′E to 58°28′ E and from 36°3′N to 36°42′ N (Fig. 1b). It has a general E–W trend and is part of the Mesozoic ophiolites that mark the boundaries of the CEIM. The Sabzevar ophiolite is situated to the north of Sabzevar town, northeastern Iran, along the Meyamey fault between the CEIM to the south and the Turan plate (i.e., the southern margin of Eurasia) to the north (Fig. 1a).

Although the Sabzevar ophiolite is highly dismembered and often characterized as a typical tectonic ophiolitic mélange (Lensch, 1980; Noghreyan, 1982; Baroz et al., 1983; Shojaat et al., 2003), schematic stratigraphic column of the studied area show that the Sabzevar ophiolite represents a complete oceanic lithospheric section and contains all the rocks that are representative of an ophiolitic sequence (Fig. 2a) (Shafaii Moghadam and Stern, 2015 and references therein). All the different lithological units and formations in the Sabzevar ophiolitic mélange are divided into two general genetic groups including: the ophiolitic (Late Cretaceous–Early Paleocene) and the post-ophiolitic (Eocene to Plio-Quaternary arc) sequences (Fig. 1b).

The ophiolitic sequence comprises of mantle peridotites, cumulate peridotites, gabbros, diabasic dikes and volcanic, sedimentary and metamorphic rocks. Mantle peridotites are the most widespread rock type in the Sabzevar ophiolite. They occur as lherzolite, clinopyroxen-bearing harzburgite, harzburgite, dunite and serpentinite. Abundant rodingitized diabase, pegmatitic gabbro, micro-gabbro and amphibolite dikes crosscut all lithologies in the mantle section. The harzburgite is the volumetrically predominant mantle peridotite and hosts dunite bodies and pyroxenite layers and veins (Rahmani, 2018). There are also large masses of podiform chromitite inside mantle sequence that are especially well-developed in the central and western parts of the Sabzevar ophiolite (Shafaii Moghadam et al., 2013).

Cumulate peridotites, gabbroic rocks and plagiogranites form the plutonic crustal sequence of the Sabzevar ophiolite. The gabbroic rocks are largely found as isolated outcrops but can be divided into layered, foliated, and isotropic gabbros. The diabasic dikes occur as both isolated intrusive bodies, which cut mantle and plutonic crustal sequences, and

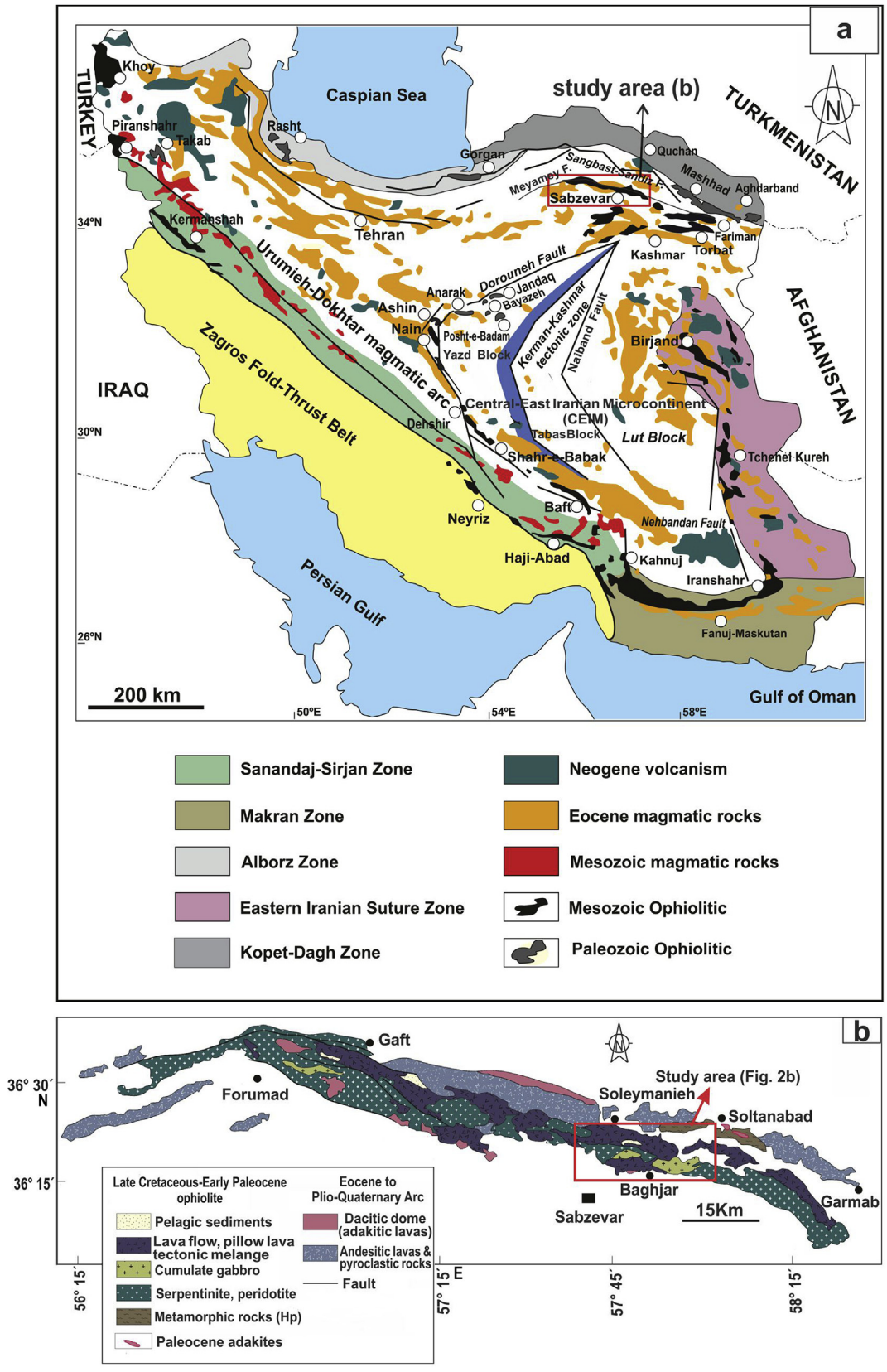

Fig. 1. (a) Main structural units of Iran and location of the study area (modified after Shafaii Moghadama et al., 2016); (b) simplified geological map of the Sabzevar ophiolite, according to Sabzevar and Forumad 1:100,000 geological maps (modified after Shafaii Moghadama et al., 2016).

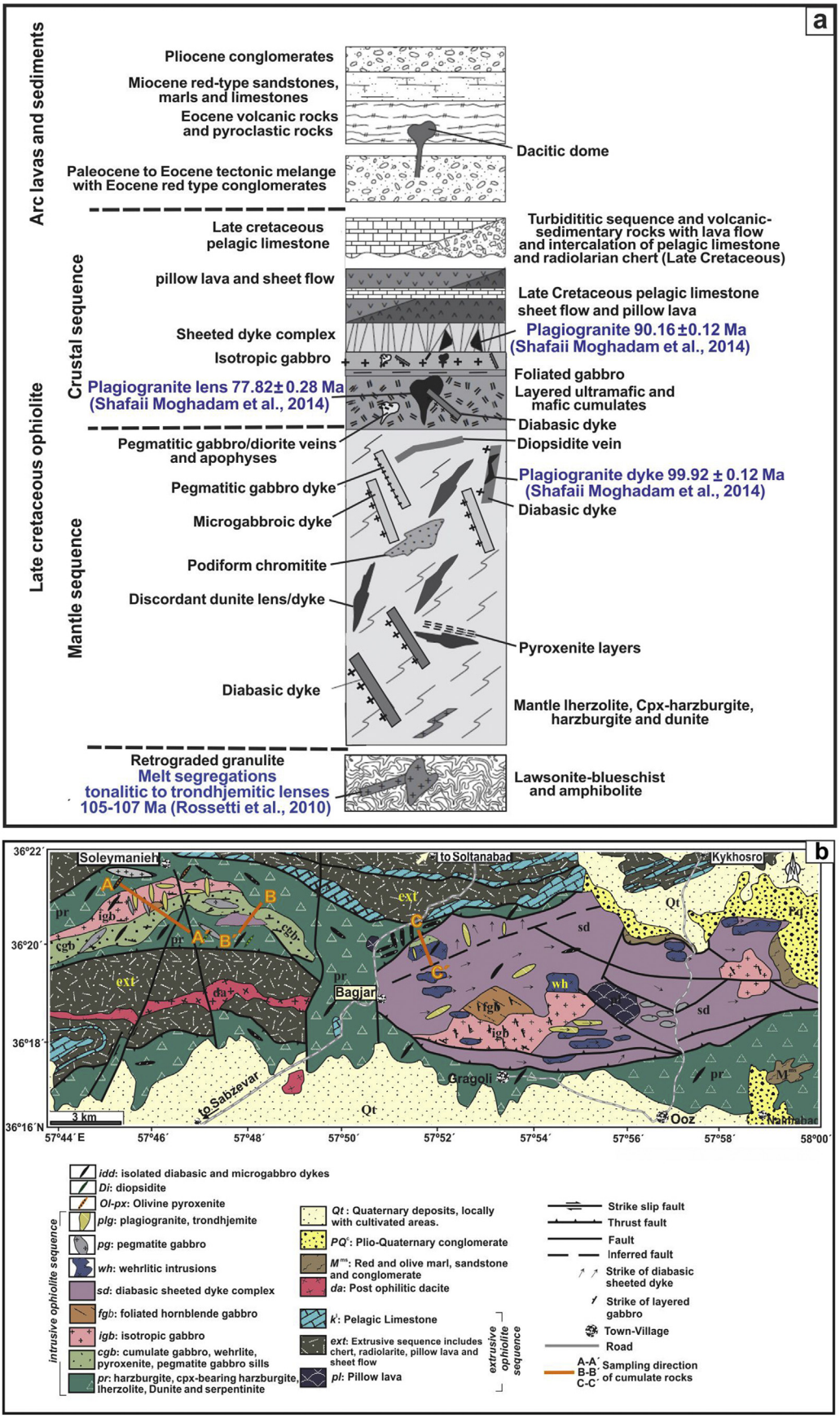

Fig. 2. (a) Schematic stratigraphic column of the Sabzevar ophiolite (modified after Shafaii Moghadam and Stern, 2015); (b) 1:75,000 geological map of the study area (modified after Khalatbari Jafari et al., 2013a).

sheeted dike complex. The extrusive sequence of the Sabzevar ophiolite consists of pillow lavas and sheet flows, which are intercalated with oceanic fossiliferous pelagic limestone and volcano-sedimentary rocks (Khalatbari Jafari et al., 2013b; Rezaei et al., 2018). The sedimentary section of the Sabzevar ophiolite comprise a sequence of turbiditic and volcano-sedimentary rocks and interlayers of oceanic fossiliferous pelagic limestone and radiolarian chert. Metamorphic rocks associated with the Sabzevar ophiolite are exposed mainly in the northern part of the area (Soltan Abad metamorphic complex, Fig. 1b) and consist of marble, greenschist, amphibolite, migmatitic mafic granulite and lawsonite-bearing blueschist (Rossetti et al., 2010; Omrani et al., 2013).

According to paleontological studies, the Sabzevar ophiolite contains Early to Late Cretaceous deep marine sediments (Lindenberg et al., 1984; Shojaat et al., 2003) and pelagic limestones between the pillow lavas contain microfossils, which show Late Campanian to Early Maastrichtian ages (~75–68 Ma), indicating upper Cretaceous age for the youngest basaltic assemblages (Shojaat et al., 2003; Khalatbari Jafari et al., 2013b; Shafaii Moghadam et al., 2014).

Geochronological data from crustal sequence rocks of the Sabzevar ophiolite show amphibole K–Ar ages of 81.2 ± 4.1 Ma and 76.8 ± 3.8 Ma for the lavas and diabases, respectively (Lensch and Davoudzadeh, 1982), as well as zircon U–Pb ages of 99.9 Ma, 90.2 Ma and 77.8 Ma for three plagiogranites (Fig. 2a), displying the crustal sequence rocks were formed over a considerable period of time in Late Cretaceous time (Shafaii Moghadam et al., 2014).

Rossetti et al. (2010) obtained zircon and titanite U–Pb ages of 107.4–105.9 Ma (Albian) for felsic segregations in the migmatitic mafic granulites (Fig. 2a) and argued that the Sabzevar granulites formed during subduction of Proto-Sabzevar Ocean in Late Early Cretaceous time. Dating of Sabzevar metamorphic rocks that are located about 40 km away from the granulite units yields ages of 58–61 Ma for amphibolites and 51 Ma for gneiss (Baroz et al., 1983; Rossetti et al., 2014). The amphibolites and associated blueschists are intruded by Late Paleocene (ca. 57 Ma; Ar–Ar muscovite and U–Pb zircon method) high–pressure adakitic granitoids, which are interpreted as slab melts emplaced at depth within the Sabzevar subduction channel (Rossetti et al., 2014). These metamorphic units are unconformably covered by non–metamorphic nummulite–bearing limestones containing rock clasts coming from both the Sabzevar metamorphics and adakitic granitoids (Omrani et al., 2013; Rossetti et al., 2014). In addition, the Sabzevar ophiolite is intruded by widespread post-ophiolite stocks and dikes of intermediate to felsic compositions that have arc signatures and show mica Ar–Ar and zircon U–Pb ages 45–47 Ma (Shafaii Moghadama et al., 2016). This age is contemporary with deposition of the nummulite–bearing limestones that unconformably cover the Sabzevar ophiolite (Rossetti et al., 2014) and indicates that the emplacement of the Sabzevar ophiolitic mélange onto the southern margin of the Turan (Eurasia) plate occurred before Early Eocene times (47–45 Ma).

According to the above paleontological and geochronological data, the Sabzevar oceanic basin existed at least since the Mid-Cretaceous and was closed during Late Paleocene–Early Eocene times possibly due to subduction of the Neotethys oceanic crust and subsequent CEIM-Eurasia plate collision. It is simultaneous with the evolution of other oceanic basins around the CEIM (Baroz et al., 1983; Arvin and Robinson, 1994; Babazadeh and De Wever, 2004; Shafaii Moghadam, 2009; Torabi, 2010; Brocker et al., 2013; Shirdashtzadeh et al., 2014).

3. Field relations and petrography

The best outcrops of the plutonic crustal sequence are located in the eastern part of the Sabzevar ophiolite (Figs. 1b and 2b). The plutonic crustal sequence consists of cumulate peridotite (Fig. 3a), layered gabbro (Fig. 3b–d), foliated gabbro (Fig. 4a) and isotropic gabbro (Fig. 4b–d), which are intruded by micro gabbro, pegmatitic to porphyritic gabbro, porphyritic diorite and plagiogranite veins, and isolated diabasic dikes (Fig. 4b–f). Plagiogranite also forms dikes and massive bodies at the top of the plutonic crustal sequence and occurs as xenoliths in the sheeted dikes. The cumulate rocks of the Sabzevar ophiolite crop out mostly in the vicinity of Soleymanieh and Baghjar villages (Figs. 1b and 2b). In this study, we selected two sections in the south of Soleymanieh and one section in the east of Baghjar (Fig. 2b).

The cumulate peridotite occurs at the base of the sequence and gradually grades upwards into layered gabbro. The layered gabbro is composed of layers up to 0.5–40 cm thick and displays well-developed

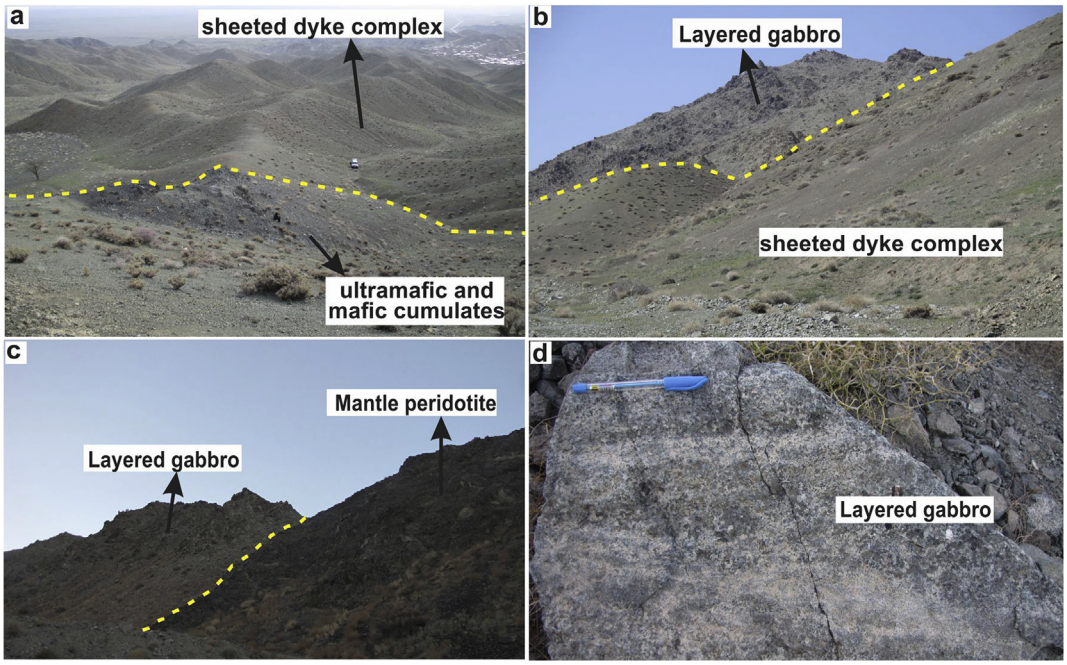

Fig. 3. Field photographs of (a) exposure of ultramafic and mafic cumulates, and sheeted dike complex, northeastern of Bagjer (C-C′ section in Fig. 2b); (b) exposure of layered gabbro and sheeted dike complex, southeastern of Soleymanieh (B-B′ section in Fig. 2b); (c) exposure of layered gabbro and mantle peridotite with a tectonized contact, southwestern of Soleymanieh (A–A′ section in Fig. 2b); (d) magmatic layering in the layered gabbro, southwestern of Soleymanieh.

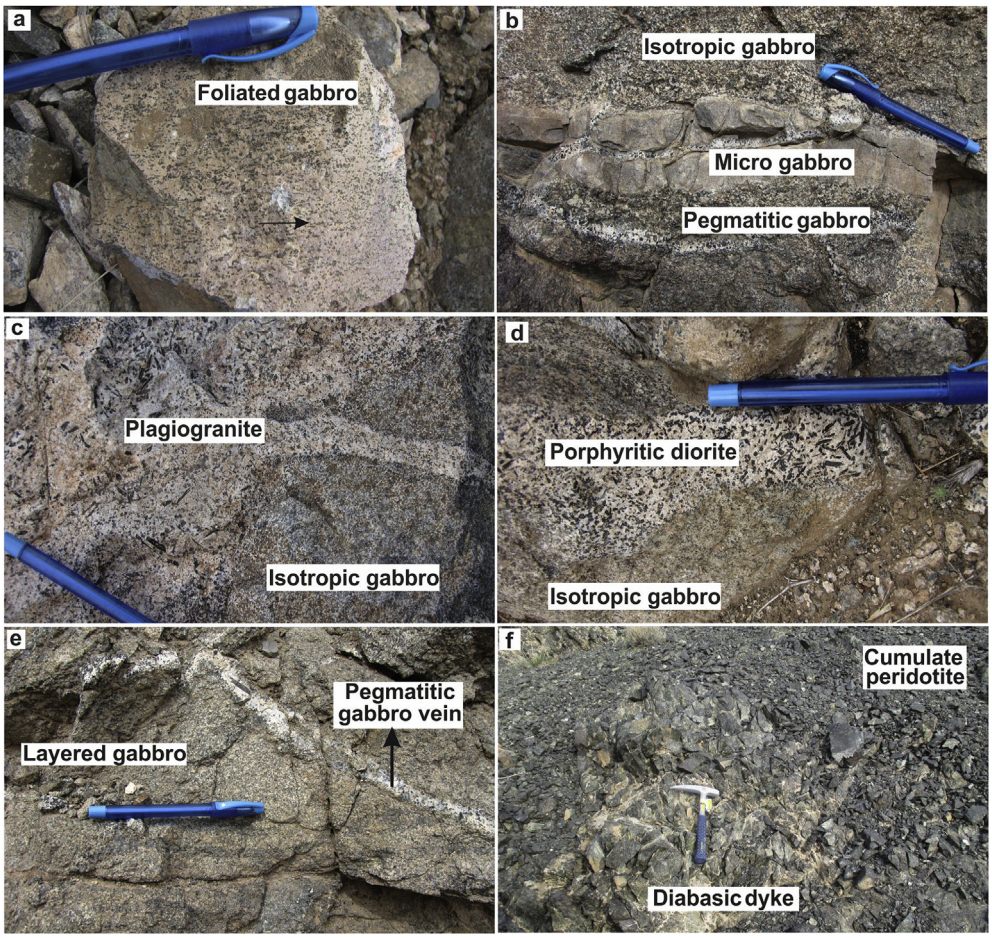

Fig. 4. Field photographs of (a) foliated gabbro, southwestern of Soleymanieh; (b–d) veins of micro gabbro, pegmatitic gabbro, porphyritic diorite and plagiogranite within isotropic gabbro, southwestern of Soleymanieh; (e) pegmatitic gabbroic vein in layered gabbro, southeastern of Soleymanieh; (f) diabasic dike within cumulate peridotite, northeastern of Bagjer.

magmatic layering and rhythmic alternations of melanocratic and leucocratic gabbro (Fig. 3d). It contains layers of medium-to coarse-grained gabbro interbedded with thin layers of fine-grained gabbro, clinopyroxenite and anorthosite. The magmatic layering gradually decreases towards the top of the sequence and layered gabbro is followed by foliated and isotropic gabbro, plagiogranite and sheeted dikes.

The ultramafic cumulates consist of plagioclase-bearing wehrlite and olivine clinopyroxenite with adcumulate, mesocumulate and heteradcumulate textures. Plagioclase-bearing wehrlite samples contain olivine (50%–55%) and clinopyroxene (35%–40%) as cumulus phases and plagioclase (7%–10%) and orthopyroxene (~5%) as intercumulus phases. The intercumulus plagioclase surrounds clinopyroxene and olivine crystals, forming a heteradcumulate texture (Fig. 5a and b). Inclusions of olivine, clinopyroxene and plagioclase in the orthopyroxene indicate their formation before orthopyroxene. In addition, fine inclusions of spinel are also seen in the olivines. The olivine clinopyroxenites consist of cumulus clinopyroxene (65%–70%) and olivine (20%–15%) and intercumulus clinopyroxene, orthopyroxene (7%–10%) and plagioclase (5%–10%) (Fig. 5c).

The mafic cumulates are represented by olivine gabbronorite, gabbronorite, amphibole gabbronorite and quartz gabbronorite with adcumulate, mesocumulate, heteradcumulate and orthocumulate textures. The olivine gabbronorites include olivine (15%–20%), clinopyroxene (35%–40%), plagioclase (30%–35%) and orthopyroxene (10%–15%). In these rocks, plagioclase occurs as both unzoned cumulus and intercumulus phases, while orthopyroxene forms intercumulus phase (Fig. 5d). In the cumulate rocks, layering is determined by variation of modal amounts of the minerals. Decreasing relative proportion of olivine is balanced by increasing amounts of orthopyroxene. The gabbronorites consist of clinopyroxene (30%–35%) as cumulus phase, and plagioclase (45%–50%) and orthopyroxene (15%–20%) as both cumulus and intercumulus phases (Fig. 5e). The amphibole gabbronorites contain 5%–10% amphibole, which surrounds clinopyroxene, orthopyroxene and plagioclase crystals as an intercumulus phase and forms heteradcumulate texture (Fig. 5f). In these rocks, plagioclase occurs as both cumulus and intercumulus phases and shows zoning. The quartz gabbronorites include about 5% quartz as an interstitial mineral and have modal compositions similar to the amphibole gabbronorite. Based on the petrographic observations, the crystallization order within the cumulate rocks of the Sabzevar ophiolite is olivine ± chromian spinel → clinopyroxene → plagioclase → orthopyroxene → amphibole.

Opaque minerals, titanite and apatite are accessory minerals in the mafic cumulates. The ultramafic and mafic cumulates of the study area were modified by moderate to low degrees of hydrothermal alteration and magmatic minerals were partly replaced by secondary minerals. The main characteristic alteration features observed in these rocks are partial to complete replacement of olivine to serpentine and magnetite (Fig. 5a–d), partial alteration of pyroxenes to amphibole (Fig. 5e) and variably alteration of plagioclase to sausserite (Fig. 5a). In some thin-sections, elongate or fibrous amphibole (uralite) forms reaction rims on pyroxenes, and is commonly associated with opaque minerals.

The pegmatitic gabbro dikes and veins that cut cumulate sequence of the Sabzevar ophiolite display cumulate textures. They are amphibole gabbronorite and contain plagioclase (5 mm size), clinopyroxene (6–12

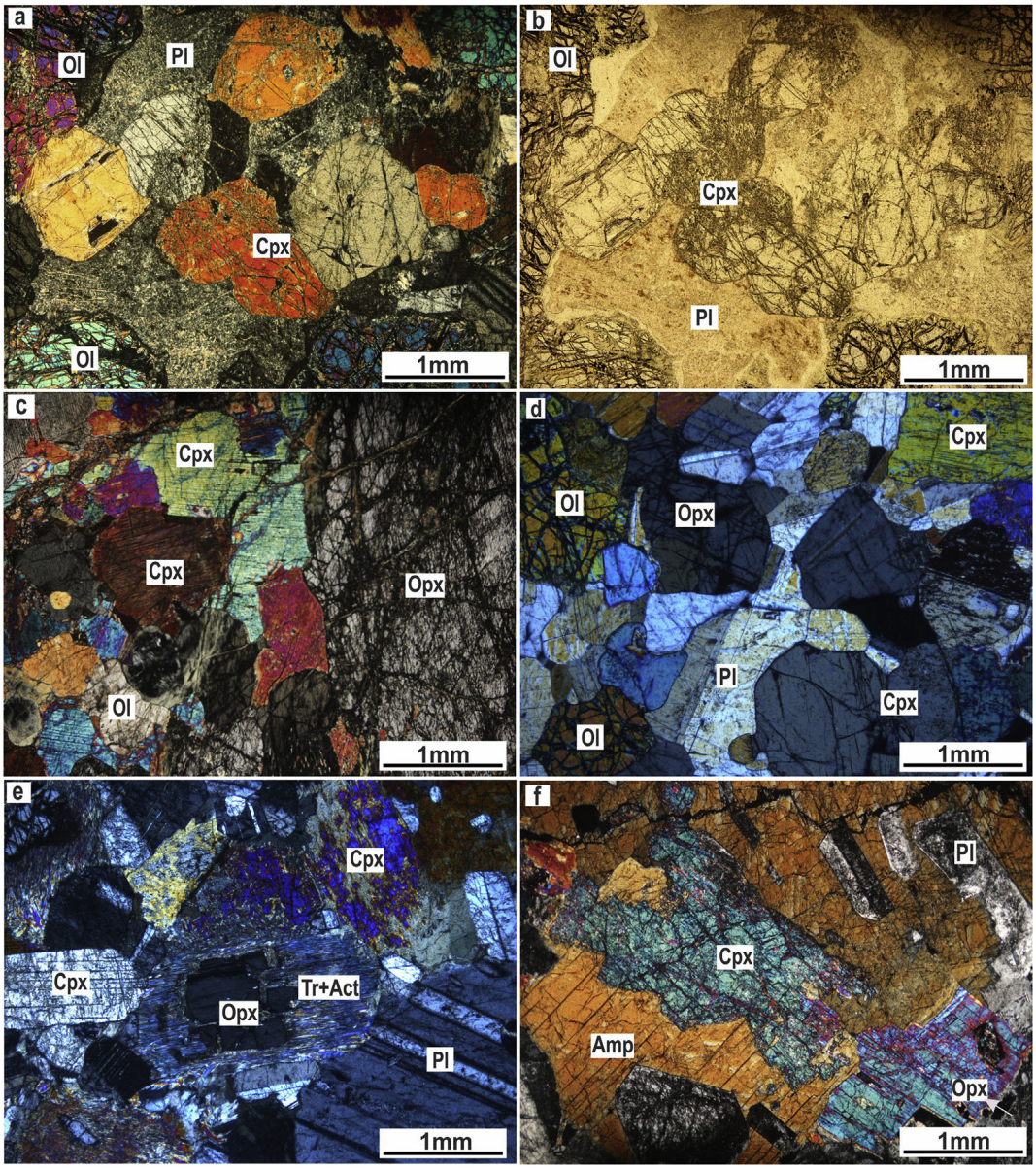

Fig. 5. Photomicrographs of ultramafic and mafic cumulates from the Sabzevar ophiolite. (a) Heteradcumulate texture in the plagioclase-bearing wehrlite (sample g-80), in which plagioclase poikilitically encloses olivine and clinopyroxene; (b) plane-polarized light of (a); (c) adcumulate texture in the olivine clinopyroxenite (sample g-41); (d) mesocumulate texture in the olivine gabbronorite (sample g-75), where plagioclase occurs between the olivine and pyroxene; (e) mesocumulate texture in the gabbronorite (sample g-10-2-2); (f) heteradcumulate texture in the amphibole gabbronorite (sample g-5), in which amphibole poikilitically encloses plagioclase and clinopyroxene. Abbreviations: Act: actinolite; Amp: amphibole; Cpx: clinopyroxene; Ol: olivine; Opx: orthopyroxene; Pl: plagioclase and Tr: tremolite. Mineral abbreviation from Whitney and Evans (2010).

mm size) and orthopyroxene (6 mm size), which are surrounded by amphibole, forming a heteradcumulate texture. In addition, samples from micro grabbroic dikes and veins inside Sabzevar cumulate sequence have microgranular and intergranular textures and contain plagioclase and clinopyroxene with a grain size of about 0.2 mm.

4. Analytical methods

Based on the petrographic study, eighteen representative samples were selected for geochemical analysis. Sixteen samples representing all lithological types were chosen from the ultramafic and mafic cumulates, along with two samples from the micro gabbroic dikes. The samples were cut into small slabs to remove the thin traces of veins. Sample powders were obtained by crushing rock slabs in a jaw crusher and powdering fragments in an agate ring mill. Bulk rock major elements were analysed by X–Ray Fluorescence (XRF) at the Instituto Andaluz de Ciencias de la Tierra (IACT, Granada, Spain) using a Bruker AXS S4 Pioneer equipped with three analyzers (LiF200, OVO-55, PET). Within–run precision (% RSD), measured by repeated analyses of USGS reference materials BHVO-2 and AGV-2 as external standards, was better than 1.5% for all elements except P (2.7%).

Bulk rock trace elements (REEs, Cs, Rb, Ba, Th, U, Pb, Nb, Ta, Sr, Zr, Hf, Y, Sc, and Cu) were analysed in solution using an Agilent 8800 QQQ Inductively Coupled Plasma–Mass Spectrometer (ICP–MS) at IACT (Granada, Spain). Sample digestion was performed following the HF/$HClO_4$ dissolution and analytical procedure described in detail by Ionov et al. (1992) and Garrido et al. (2000). Bulk rock trace element concentrations were determined by external calibration, except for Hf that was calculated using Zr measured by XRF and the chondritic Zr/Hf ratio. Accuracy of the ICP–MS analyses was assessed from the results obtained

for the international rock standards JP–1, UBN, PM–S, MRG-1 and DNC–1a, analysed as an unknown during the same analytical runs as the Sabzevar ophiolite samples. Our results (Supplementary Table 2) show good agreement with working values for these reference materials (Flanagan, 1984; Govindaraju, 1994; Dulski, 2001; Deschamps et al., 2010; Debret et al., 2013; GeoReM database: http://georem.mpch-mainz.gwdg.de).

In situ trace element analyses of clinopyroxenes were carried out by laser–ablation (LA) ICP–MS. Analyses were performed at IACT (Granada, Spain) using a Agilent 8800 QQQ instrument coupled with a Photon Machine Analyte G2 system equipped with a 193 nm wavelength excimer laser. In each analytical setup, reference sample BIR–1G (basaltic glass reference sample) was analysed as an external standard. Results show good agreement with working values for this reference sample (GeoReM database: http://georem.mpch-mainz.gwdg.de; Govindaraju, 1994) except for Cs, Rb and U (Table 1).The laser was fired using an energy density of 10.8 J/cm^2 at a frequency of 10 Hz and using a spot size of 85 μm. Data were corrected using the Iolite software of Paton et al. (2011).

5. Mineral chemistry

5.1. Major element compositions

In a previous paper (Rahmani et al., 2017), we presented major element chemical characteristics of minerals from the studied ultramafic and mafic cumulate rocks. It shows that the forsterite (Fo) contents of olivine in the ultramafic and mafic cumulate samples range of 81.6%–89.8% and 80.5%–84.1%, respectively. The composition of clinopyroxenes from ultramafic cumulate samples is diopside ($En_{50.7–47.1}Fs_{7.0–4.1}Wo_{48.0–42.3}$), whereas clinopyroxenes from the mafic cumulates show weak Fe enrichment ($En_{49.1–40.6}Fs_{14.2–6.0}Wo_{46.4–41.5}$) with differentiation and have composition of diopside to augite. Clinopyroxenes have high Mg number [Mg# = 100 × Mg/(Mg + Fe^{2+})] (91–98 and 77–96 for ultramafic and mafic cumulates, respectively). Orthopyroxenes are enstatite and Mg# of them range from 90–93 in the ultramafic and 75–89 in the mafic cumulates. Compositionally, plagioclase ranges of anorthite to bytownite ($An_{93.0–91.4}$ to $An_{92.7–87.6}$) for the ultramafic and mafic cumulates, respectively. According to nomenclature of the amphibole-supergroup minerals from Hawthorne et al. (2012), the composition of amphibole from Sabzevar cumulate rocks ranges from Ti-rich magnesio-ferri-hornblende to magnesio-ferri-hornblende.

5.2. Trace element compositions of clinopyroxenes

Trace element data of clinopyroxenes from the plagioclase-bearing wehrlite, olivine gabbronorite and pegmatitic gabbro dike are given in Table 1. The chondrite–normalized REE patterns of the clinopyroxenes from different lithologies are similar. The clinopyroxenes have low REE contents and highly fractionated chondrite–normalized REE patterns (Fig. 6a and c) with a strong LREE depletion compared to MREE and HREE [$(La/Sm)_N$ = 0.10–0.27 and $(La/Yb)_N$ = 0.08–0.22]. Normalized REE concentrations of the clinopyroxenes uniformly increase from LREE to MREE and have an almost flat pattern in the MREE to HREE region [$(Gd/Yb)_N$ = 1–1.25]. Clinopyroxenes from the plagioclase-bearing wehrlite and olivine gabbronorite samples show very small negative Eu anomalies (Eu/Eu* = 0.90–0.96) that indicate their precipitation from the melt that was little fractionated by plagioclase crystallization (e.g., Greene et al., 2006; Drouin et al., 2009; Gahlan et al., 2012).

Table 1
Trace elements and REE concentrations of clinopyroxene in cumulate samples from the Sabzevar ophiolite.

Lithology	Plagioclase bearing wehrlite			Olivine gabbronorite				Pegmatitic gabbro	LA-ICP-MS standard		
Sample No.	g-80	g-80	g-80	g-75	g-75	g-62	g-62	g-32	BIR-1G	BIR-1G (GeoReM database)	RSD (%)
Point No.	1	2	3	1	2	1	2	1	n = 5	mean	
Li (ppm)	0.62	0.68	0.55	0.66	0.69	1.31	1.17	1.27	3.2	3.2	1
Sc	38.4	44.1	41.7	45.8	41.8	37.1	41.1	52.4	44.1	43.0	2
Cs	0.012	0.015	0.002	0.048	0.002	0.029	0.11	0.68	0.057	0.005*	1040
Rb	0.027	0.031	0.009	0.028	0.017	0.21	0.38	5.5	0.18	0.25*	−29
Ba	0.057	0.047	0.023	0.056	0.068	0.24	0.24	0.099	6.5	7.1	−9
Th	0.002	0.001	0.002	0.001	0.002	0.013	0.030	0.005	0.029	0.032	−8
U	0.0000	0.0007	0.0009	0.0006	0.0003	0.057	0.011	0.0003	0.019	0.010	93
Nb	0.001	0.003	0.002	0.004	0.004	0.008	0.005	0.005	0.51	0.55	−7
Ta	0.0002	0.0002	0.0004	0.0003	0.0007	0.0006	0.0006	0.0005	0.036	0.036	−1
La	0.040	0.070	0.051	0.055	0.060	0.088	0.14	0.077	0.60	0.62	−2
Ce	0.21	0.37	0.24	0.28	0.29	0.30	0.54	0.42	1.9	1.9	−1
Pb	0.003	0.020	0.010	0.010	0.016	0.14	0.037	0.023	3.4	3.1	9
Pr	0.051	0.092	0.060	0.075	0.070	0.059	0.11	0.11	0.36	0.37	−4
Sr	4.3	4.7	4.8	4.1	4.4	4.3	4.4	4.1	110.0	109.0	1
Nd	0.34	0.61	0.39	0.49	0.45	0.38	0.69	0.77	2.2	2.4	−9
Zr	1.2	2.1	1.3	1.6	1.7	1.3	2.6	2.4	14.0	14.0	0
Hf	0.066	0.12	0.069	0.087	0.079	0.12	0.12	0.14	0.57	0.58	−2
Sm	0.23	0.41	0.26	0.35	0.33	0.21	0.42	0.47	1.1	1.1	0
Eu	0.091	0.16	0.11	0.13	0.13	0.090	0.15	0.18	0.52	0.53	−2
Gd	0.40	0.57	0.45	0.58	0.51	0.40	0.64	0.81	1.8	1.9	−2
Tb	0.073	0.13	0.090	0.11	0.098	0.069	0.12	0.16	0.36	0.36	−1
Dy	0.52	0.88	0.60	0.83	0.69	0.51	0.84	1.1	2.5	2.5	−1
Y	2.7	4.5	3.1	4.1	3.7	3.0	4.3	5.2	14.6	15.6	−6
Ho	0.11	0.20	0.13	0.17	0.15	0.11	0.18	0.25	0.57	0.56	2
Er	0.31	0.52	0.36	0.47	0.42	0.31	0.52	0.71	1.7	1.7	1
Tm	0.040	0.069	0.047	0.066	0.058	0.043	0.070	0.11	0.24	0.25	−3
Yb	0.27	0.42	0.30	0.43	0.37	0.29	0.42	0.67	1.6	1.7	−2
Lu	0.036	0.061	0.045	0.060	0.056	0.039	0.058	0.084	0.25	0.25	−1
Eu/Eu*	0.91	0.90	0.96	0.91	0.93	0.96	0.90	0.87			
$(La/Sm)_N$	0.11	0.11	0.12	0.098	0.11	0.27	0.20	0.10			
$(La/Yb)_N$	0.10	0.12	0.12	0.089	0.11	0.21	0.22	0.080			
$(Gd/Yb)_N$	1.2	1.2	1.2	1.1	1.1	1.1	1.3	1.0			

N: normalized to chondrite after Sun and McDonough (1989); Eu/Eu* = $Eu_N/(Sm_N \times Gd_N)^{0.5}$.
GeoReM database: http://georem.mpch-mainz.gwdg.de; *: values from Govindaraju (1994); RSD and minor elements, using (a)(%): relative standard deviation (percentage).

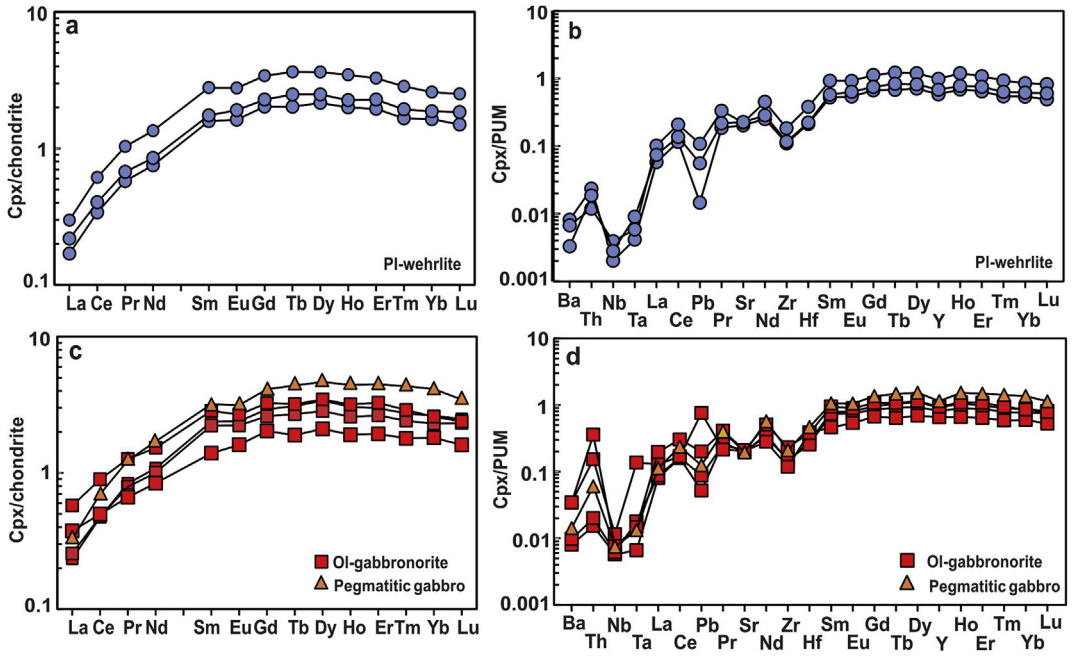

Fig. 6. Chondrite-normalized REE and PUM-normalized trace element patterns of clinopyroxene (Cpx) from the Sabzevar ophiolite cumulate rocks, (a and b) plagioclase-bearing wehrlite; (c and d) olivine gabbronorite and pegmatitic gabbro. Normalizing values from Sun and McDonough (1989). PUM: primitive upper mantle.

Clinopyroxene from the pegmatitic gabbro dike has larger negative Eu anomalies (Eu/Eu* = 0.87), which may suggest higher degrees of crystal fractionation for pegmatitic gabbros. The investigated clinopyroxenes display similar primitive upper mantle (PUM)-normalized trace element patterns with a flat pattern in MREE to HREE and negative anomalies in Zr, Nb, Ba and Pb compared to the adjacent elements. They also show a marked depletion in trace element concentrations relative to PUM, except for MREE concentrations in one plagioclase-bearing wehrlite sample (Fig. 6b and d). Normalisation to PUM reveals that in all clinopyroxenes, Nb, Zr, Hf and Ta are depleted relative to HREE and Y. The clinopyroxenes also show slight Sr negative anomaly that is in accordance with crystallization of interstitial plagioclase in these rocks.

6. Whole rock geochemistry

Representative whole rock major and trace element concentrations of the ultramafic and mafic cumulates and micro grabbroic samples are presented in Supplementary Table 1.

6.1. Major element compositions

The LOI values range from 1.73 wt.% to 6.12 wt.% for the ultramafic cumulate and from 0.54 wt.% to 5.07 wt.% for the mafic cumulate samples. These values vary depending on the abundance of primary and secondary alteration phases (serpentine group minerals, epidote, calcite, chlorite and amphibole). The geochemical data show that the SiO_2 content is 40.64–43.38 wt.% in plagioclase-bearing wehrlite and 45.93–53.51 wt.% in olivine clinopyroxenite and mafic cumulates. Sabzevar ultramafic and mafic cumulate samples characterized by low TiO_2 (0.18–0.57 wt.%), P_2O_5 (<0.05 wt.%), K_2O (0.01–0.51 wt.%) and total alkali contents (0.12–3.04 wt.%). In the discriminate diagram based on a variation of TiO_2 versus mafic index [$FeO^t/(FeO^t + MgO)$] (Serri, 1981), Sabzevar cumulate samples mostly plot in the low-Ti ophiolite field (Fig. 7a).

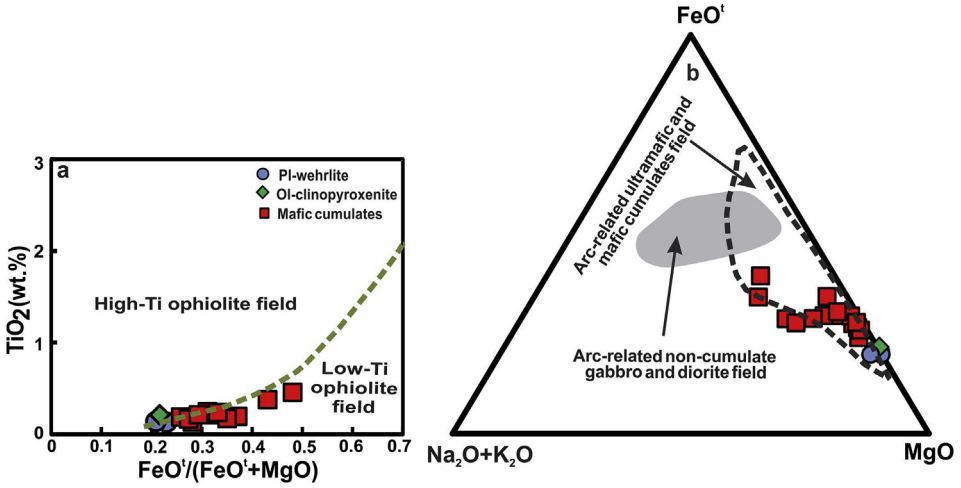

Fig. 7. Classification of cumulate rocks from the Sabzevar ophiolite based on the major and minor elements, using (a) TiO_2–$FeO^t/(FeO^t + MgO)$ diagram (after Serri, 1981); (b) ternary AFM diagram (after Irvine and Baragar, 1971). Fields of cumulate and non-cumulate rocks are from Beard (1986).

The studied rocks range from highly magnesian (31.48–28.77 wt.%) in plagioclase-bearing wehrlite to less magnesian (20.42–6.41 wt.%) in olivine clinopyroxenite and more evolved rocks such as olivine gabbronorite, gabbronorite, amphibole gabbronorite and quartz gabbronorite which have high CaO (10.64–16.66 wt.%) and Al_2O_3 (8.29–20.77 wt.%) contents. Fig. 8 shows selected major element variations of the ultramafic and mafic cumulates with MgO (assumed here as a differentiation index). In general, there is a positive correlation between Fe_2O_3 and MgO contents, whereas SiO_2, Al_2O_3, Na_2O, CaO and TiO_2 values of majority of studied cumulate rocks increase with decreasing MgO contents and only show minor disturbances, which can be explained by the alteration of minerals and/or cumulate nature of these rocks. The general trend from Mg-rich to Ca- and Al-rich cumulates is as a consequence of magmatic accumulation of olivines, clinopyroxenes and plagioclase and the progressive differentiation in the Sabzevar ophiolite magma chamber. The major element compositions of Sabzevar cumulate rocks in the ternary ($FeO + Fe_2O_3$)–($Na_2O + K_2O$)–MgO (AFM) diagram of Irvine and Baragar (1971) overlap with field of arc-related ultramafic and mafic cumulates of Beard (1986) (Fig. 7b).

The micro grabbroic dike samples have 50.88–51.53 wt.% SiO_2, 7.77–12.63 wt.% MgO, 13.28–17.53 wt.% Al_2O_3 and 10.23–10.95 wt.% CaO values. They contain low TiO_2 (0.55–0.59 wt.%), P_2O_5 (0.04–0.05 wt.%) and K_2O (0.07–0.63 wt.%) contents.

6.2. Trace element compositions

Chondrite-normalized REE patterns for the ultramafic and mafic cumulate samples are parallel and increase in abundance systematically from plagioclase-bearing wehrlite, olivine gabbronorite and olivine clinopyroxenite [(0.4–5) × chondrite] through gabbronorite, amphibole gabbronorite and quartz gabbronorite [(1–6) × chondrite] (Fig. 9a, c, e and g). This suggest that the different rock types are related to each other by differentiation of the same primary magma (e.g., Kelemen et al., 1997; Marchesi et al., 2006). The REE patterns show increasing trend from La to Sm, positive Eu anomaly (Eu/Eu* = 1.06–1.54) and an almost flat pattern from MREE to HREE region [$(Gd/Yb)_N$ = 1–1.17]. The positive Eu anomaly in these rocks is due to the accumulation of calcic plagioclases and clearly reflect their cumulate nature (e.g., Berger et al., 2001; Greene et al., 2006). Moreover, the flat HREE patterns shown by the samples are in accordance with the existence of considerable amounts of clinopyroxene (e.g., Berger et al., 2001). The plagioclase-bearing wehrlites, olivine clinopyroxenite, olivine gabbronorites (except for sample g-62) and gabbronorites display noticeably LREE depletion relative to MREE and HREE [$(La/Sm)_N$ = 0.25–0.55 and $(La/Yb)_N$ = 0.19–0.43] (Fig. 9a, c, and e). The REE patterns progressively flatten with increasing REE abundance in the amphibole gabbronorites and quartz gabbronorites [$(La/Sm)_N$ = 0.64–0.75 and $(La/Yb)_N$ = 0.60–0.76] (Fig. 9g). Sample g-62 has higher LREE abundances compared to other olivine gabbronorite samples and displays lower LREE depletion relative to MREE and HREE [$(La/Sm)_N$ = 0.8 and $(La/Yb)_N$ = 0.8].

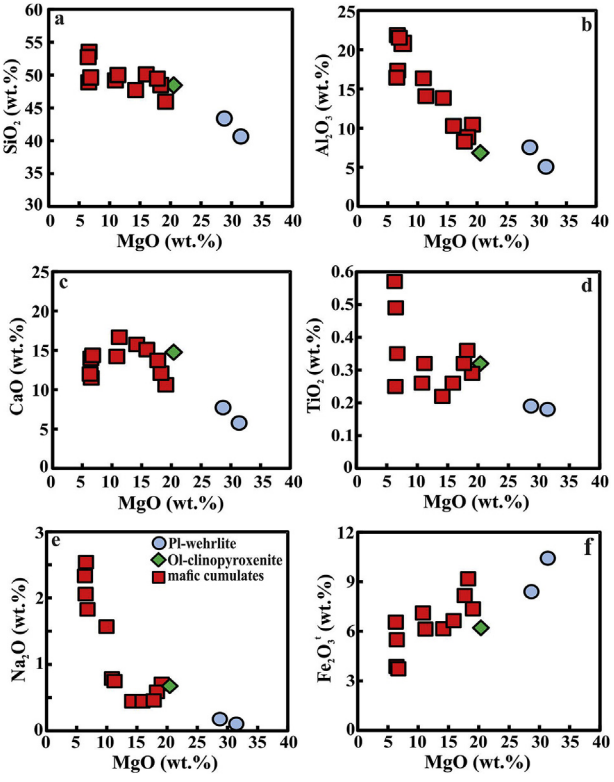

Fig. 8. Plots of selected major elements of ultramafic and mafic cumulate from the Sabzevar ophiolite against MgO as a differentiation index.

The most abundant trace element in the studied cumulate rocks is Sr, from 14.50 to 74.50 ppm in the ultramafic, and from 55.26 to 233.20 ppm in the mafic cumulate rocks and increases markedly with decreasing MgO, probably due to higher amount of plagioclase in the mafic cumulates (e.g. Grove and Baker, 1984; Beard, 1986; Kelemen et al., 2003). Sc shows considerable variation in both ultramafic (17.1–50.9 ppm) and mafic (22.2–51.9 ppm) cumulates, which most likely correlates with the fractionation of clinopyroxene (e.g. Ross et al., 1954; Borisenko, 1967; Ballantyne, 1992). The investigated cumulate samples display similar PUM-normalized trace element patterns with a flat pattern in MREE to HREE, positive anomalies in Sr, Pb and Eu and negative anomalies in Zr and Nb relative to the adjacent elements (Fig. 9b, d, f and h). The general trend of the spider diagrams exhibit slight enrichment in the LILEs relative to the HFSEs and enrichment of Sr compared to PUM (except in one plagioclase-bearing wehrlite sample g-51).

The plagioclase-bearing wehrlite, olivine clinopyroxenite, olivine gabbronorite and gabbronorite samples are mostly depleted in LREEs, LILEs such as Cs, Rb and Ba, as well as some of HFSEs including U, Th, Ta, Zr, Hf and Nb relative to PUM (Fig. 9b, d and f). The low abundances of the incompatible trace elements can be result of the high proportion of cumulus minerals and the low amounts of intercumulus liquid in the magma chamber (e.g., Parlak et al., 1996, 2000, 2002; Berger et al., 2001). The incompatible trace element values gradually increase in amphibole gabbronorite and quartz gabbronorite samples (Fig. 9h). It could represent the intercumulus liquid becoming more evolved as other phases (olivine, clinopyroxene and plagioclase) are progressively fractionated. The trace element concentrations of the remaining liquid should increase with this fractionation. It is noteworthy that the pegmatitic gabbro samples have chondrite-normalized REE and PUM-normalized trace element patterns similar to the amphibole gabbronorites (more evolved cumulate rocks) (Fig. 9g and h).

The micro grabbroic dike samples exhibit REE enrichment compared to the chondrite composition [(5–10) × chondrite] (Fig. 9g). Chondrite-normalized REE patterns of them indicate slightly LREE depletion with respect to MREE and HREE [$(La/Sm)_N$ = 0.65–0.75 and $(La/Yb)_N$ = 0.62–0.78], negligible positive Eu anomaly (Eu/Eu* = 1.08–1.12) and an almost flat pattern from MREE to HREE region [$(Gd/Yb)_N$ = 1.11–1.14]. These samples have low Zr/Hf ratios (28.30–30.36) and PUM–normalized trace elements diagram of them show Nb and Pb negative anomalies and Sr positive anomaly relative to neighboring elements (Fig. 9h).

7. Discussion

7.1. Evaluation of the alteration and crystal accumulation effects on whole rock composition

The examined cumulate rocks are affected by various degrees of alteration, between low to modrate, which led to different extent of replacement of the primary igneous phases and an increase in the loss on ignition (LOI = 0. 54–6.12 wt.%). The plagioclase-bearing wehrlites and

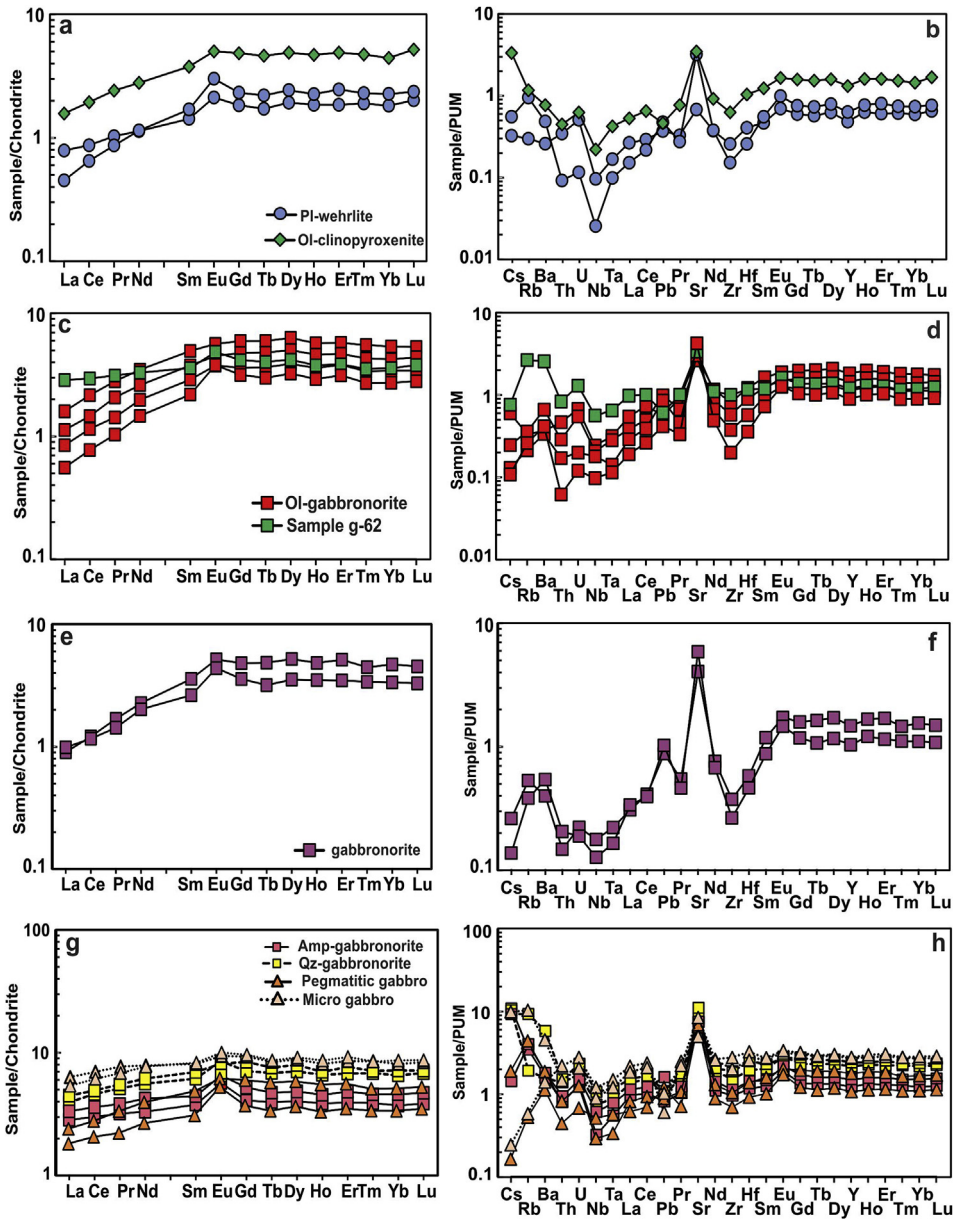

Fig. 9. Chondrite-normalized REE and PUM-normalized trace element patterns of cumulate rocks and micro grabbroic dike samples within cumulate sequence of the Sabzevar ophiolite; (a and b) plagioclase-bearing wehrlite and olivine clinopyroxenite; (c and d) olivine gabbronorite; (e and f) gabbronorite; (g and h) amphibole gabbronorite, quartz gabbronorite, pegmatitic gabbro and micro grabbroic dike samples. Normalizing values from Sun and McDonough (1989). The detection limit was below 0.000001 ppm for all elements except for Rb and Zr which were 0.000005 ppm and 0.000008 ppm, respectively. PUM: primitive upper mantle.

one of olivine gabbronorite sample have the highest amounts of LOI (3.55–6.12 wt.%), which is mainly due to partial to complete alteration of olivine to serpentine. The alteration degree in the other mafic cumulates is weak and LOI content of them is not significant and never exceeds 2.3 wt.%. During alteration, LIL elements, LREE and many major elements generally show some degrees of mobilization while HFS elements (e.g., Ti, P, Zr, Y, Sc, Nb, Ta, Hf and Th), MREE and HREE are approximately immobile and retain the typical igneous concentration levels and are therefore suitable for petrogenetic and geotectonic investigation (Rollinson, 1993; Jiang, 2000; Salvi et al., 2000; Jiang et al., 2003; Karakaya, 2009). In addition, investigations on the behavior of isovalent trace elements (Y, REEs, Zr and Hf) in magmatic and aqueous systems (Bau, 1996) have shown that in pure silicate melts, elements with similar charge and radius such as the Y–Ho and Zr–Hf twin pairs show coherent behavior and retain chondritic ratio. In contrast, in aqueous systems and their precipitates, Y–Ho and Zr–Hf twin pairs show non-coherent behavior. Sabzevar cumulate rocks have always well preserved the primary magmatic textures (Fig. 5) and show minor chemical disruption of the major element contents (Fig. 8). Moreover, plotting of the samples on Zr vs. Hf, Y vs. Ho and La vs. La/Yb diagrams (as indicators of alteration and fractionations) and calculating the correlation coefficients (r^2) show these twin pairs have a good linear correlations ($r^2 = 0.85–0.99$). These features, along with the parallelism of most trace element patterns (Fig. 9), indicate that few of the geochemical characteristics of the studied cumulate rocks have been modified by alteration and they significantly preserve the characteristics of primary igneous.

The major and trace element compositions of cumulate rocks are mainly controlled by modal proportions and assemblages of cumulus minerals and intercumulus phases in these rocks. Investigations on the trace elements composition of minerals from mafic and ultramafic cumulates (Otamendi et al., 2016) indicated that olivine and Cr–Al spinel are the major hosts of Ni and Co. In addition, olivine is also a host for Li, Sc and U, while spinel is also repository of Cr, V and Zn. With decreasing of modal proportion of olivine, orthopyroxene becomes a major phase for those trace elements hosted by olivine. These investigations revealed that majority of trace elements including LILE (Rb, Ba, Sr, U, Th), HFSE (Nb, Ta, Zr, Hf) and REEs are highly incompatible with most of the silicates and oxides. Clinopyroxene is the predominant host for Sc, MREE and HREE, and to a variable degree, Ti and Cr. Plagioclase is the main host of Sr and Pb, as well as Ba, Eu, La and Ce. Inaddition, crystallization of

magmatic amphibole in a hydrous cumulate system fractionates Ti, Y, MREE and HREE from other incompatible elements. In contrast, late magmatic to subsolidus amphibole has no effect on the differentiation of a primary magma.

Primitive mantle and chondrite-normalized trace and rare earth element patterns of Sabzevar ultramafic and mafic cumulate rocks are highly similar, suggesting that these rocks were generated by differentiation of the same primitive magma. The trace and rare earth element contents progressively increase from plagioclase-bearing wehrlite, olivine gabbronorite (except for sample g-62) and olivine clinopyroxenite through gabbronorite, amphibole gabbronorite and quartz gabbronorite, in accordance with increasing modal abundances of clinopyroxene and plagioclase as cumulus and amphibole as intercumulus phases.

Olivine gabbronorite sample g-62 has higher LREE, LILE, Nb, Ta and Zr abundances compared to other olivine gabbronorite samples, while its MREE and HRRE contents are similar to other olivine gabbronorite samples (Fig. 9c and d). Generally, different REE and trace element patterns in cumulate rocks reflect variations in the proportion of cumulus phases (olivine, pyroxene and plagioclase) and small amounts of intercumulus melt, which is highly enriched in incompatible elements compared to cumulate phases and essentially control the whole-rock composition despite being small amounts (Berger et al., 2001; Borghini and Rampone, 2007; Allahyari et al., 2014; Tanirli and Rizaoglu, 2016). Sample g-62 largely consists of olivine and clinopyroxene and has higher MgO contents (19.12 wt.%) relative to other olivine gabbronorite samples (18.33–15.22 wt.%). Therefore, it is difficult for variations in mineral proportion to explain its LREE, LILE, Nb, Ta and Zr abundances. These abundances are possibly related to the proportion of intercumulus minerals, which crystallized in equilibrium with a trapped melt fraction with geochemical characteristics similar to parental melt.

7.2. Inferred parental melt

7.2.1. Petrography and major elements geochemistry approach

The petrographical and geochemical characteristics show that Sabzevar cumulate rocks formed by fractional crystallization and differentiation. The general differentiation trend is from highly magnesian ultramafic cumulates to mafic cumulates rich in Al_2O_3 and CaO (Supplementary Table 1; Fig. 8b and c). Whole-rock geochemical compositions indicate that the ultramafic and mafic cumulate samples can be classified as low-Ti ophiolite related rocks (Fig. 7a). By using the fractionation trends of both gabbroic rocks, dikes and basalts from ophiolitic suites (Miyashiro, 1973, 1975; Serri, 1981) and distinct magma types of the modern oceanic setting (Beccaluva et al., 1989), ophiolites have been grouped into high-Ti, low-Ti and very low-Ti ophiolite types. The High-Ti ophiolites disply typical characteristics of MORB-like magmas, occurring at mid-ocean ridges and well developed marginal basins, while the low-Ti and very low-Ti ophiolites are comparable to IAT and boninitic-like magmas, respectively, typically form in intra-oceanic island arc settings (Beccaluva et al., 1989). In arc-related ophiolites, clinopyroxene and orthopyroxene are common minerals in crustal plutonic rocks (e.g., Elthon et al., 1982; Beccaluva et al., 1983; Parlak et al., 1996, 2002), but the crystallization order of minerals differs in IAT and boninitic magmas. The crystallization order in IAT magmas is: olivine ± Cr-spinel → clinopyroxene → plagioclase → orthopyroxene, whereas in boninitic magmas is: olivine ± Cr-spinel → clinopyroxene → orthopyroxene → plagioclase. The petrographic observations show crystallization order in the studied rocks is olivine ± chromian spinel → clinopyroxene → plagioclase → orthopyroxene → amphibole, correspond to crystallization order observed in IAT magmas.

Pearce and Norry (1979) demonstrated that Ti contents of clinopyroxene indicate the degree of depletion of the mantle source and the Ti activity of the parental melt. Geochemical studies indicate that clinopyroxenes from MORB cumulates have 0.6–1.4 wt.% TiO_2 (Elthon, 1987; Niu et al., 2002), while those from IAT and boninitic cumulates have 0.18–0.54 wt.% and <0.15 wt.% TiO_2 contents, respectively (Greene et al., 2006; Tribuzio et al., 2008). TiO_2 contents of clinopyroxenes from Sabzevar cumulate rocks vary from 0.14 wt.% to 0.52 wt.% (Rahmani et al., 2017) and are comparable to those from IAT cumulates, which crystallized from a low Ti melt (e.g. Greene et al., 2006). Other studies have shown that partial melting and remelting of mantle peridotites can lead to the removal of Ti from mantle clinopyroxenes and the generation Ti-poor magmas (Duncan and Green, 1980; Hébert and Laurent, 1990). Accordingly, it is suggested that Sabzevar cumulate rocks have been crystallized from a low Ti parental melt, which formed by partial melting of already depleted mantle peridotite. Low Ti magma was the source for the ophiolitic basalts and plutonic rocks that formed in SSZ settings (Camuzcuoğlu et al., 2017 and references therein).

Experimental results show that crystallization of plagioclase is repressed relative to olivine and clinopyroxene in water-rich tholeiitic magmas (Gaetani et al., 1993; Falloon and Danyushevsky, 2000; Koepke et al., 2004; Berndt et al., 2005; Feig et al., 2006; France et al., 2013). This is favorable to cumulate rocks from SSZ settings, where hydrous parental melts are generated by fluid-increased melting due to the subducted slab (Beccaluva and Serri, 1988; Shervais et al., 2004; Koepke et al., 2009). Early crystallization of clinopyroxene relative to plagioclase in combination with the presence of primary magmatic amphibole in Sabzevar cumulate rocks cannot be explained easily by fractional crystallization of dry MORB melts, where plagioclase crystallizes before clinopyroxene, and suggests that investigated rocks are cumulates derived from melts that were richer in H_2O compared to MORB parent melts (e.g., Liu et al., 2014 and references therein).

7.2.2. Trace elements geochemistry approach

In Fig. 10, the REE patterns and spider diagrams of Sabzevar ultramafic and mafic cumulate rocks are compared to those from crustal cumulates from mid ocean ridges (Ross and Elthon, 1997; Hart et al., 1999) and island arc (Greene et al., 2006), as well as fore-arc (boninitic) ultramafic and depleted mafic crustal cumulates from the Sarve-Abad ophiolites (Iran) and the Massif du Sud ophiolite (New Caledonia), respectively (Marchesi et al., 2009; Allahyari et al., 2014). Sabzevar cumulate rocks display chondrite-normalized REE patterns, which are very different from the fore-arc boninitic crustal cumulates, but are comparable with ocean ridge and island arc crustal cumulates (Fig. 10a and c). However, comparing both the spider and REE diagrams (Fig. 10a–d) clearly shows that Sabzevar cumulate samples have characteristics most similar to island arc crustal cumulates. On the other hand, chondrite-normalized REE patterns of clinopyroxenes from Sabzevar ultramafic and mafic cumulates show depletion in REE concentrations compared to clinopyroxenes from ocean ridge cumulates (Fig. 11a) and overlap with clinopyroxenes from island arc and boninitic cumulates (Fig. 11b and d). Although, increasing trend from LREE to MREE and flat pattern in the MREE to HREE region show that clinopyroxenes from Sabzevar cumulates have close similarities with those from island arc crustal cumulates (Fig. 11b) and are different from clinopyroxenes from boninitic and fore-arc depleted mafic cumulates (Fig. 11c and d).

Typically, the magmatic affinity of the parental melt of cumulus rocks can be determined by chemical composition of igneous clinopyroxenes, using suitable mineral–liquid distribution coefficients to calculate the trace element composition of equilibrium melt (e.g., De Hoog et al., 2011). Clinopyroxenes, which form during the early crystallization stage of a mantle-derived magma preserve important information regarding the composition of the parental melt and the melt source (Muravyeva et al., 2014). It is important to choose clinopyroxenes with the best-preserved igneous composition that were not affected by late post-cumulus crystallization. In order to minimize these effects, we have only considered the trace element abundances measured in cores of large cumulus clinopyroxenes from plagioclase-bearing wehrlite (samples g80-1 and g80-3) and olivine gabbronorite samples (samples g-75-2 and g-62-1), which have the lowest REE concentrations (i.e., the lowest Yb

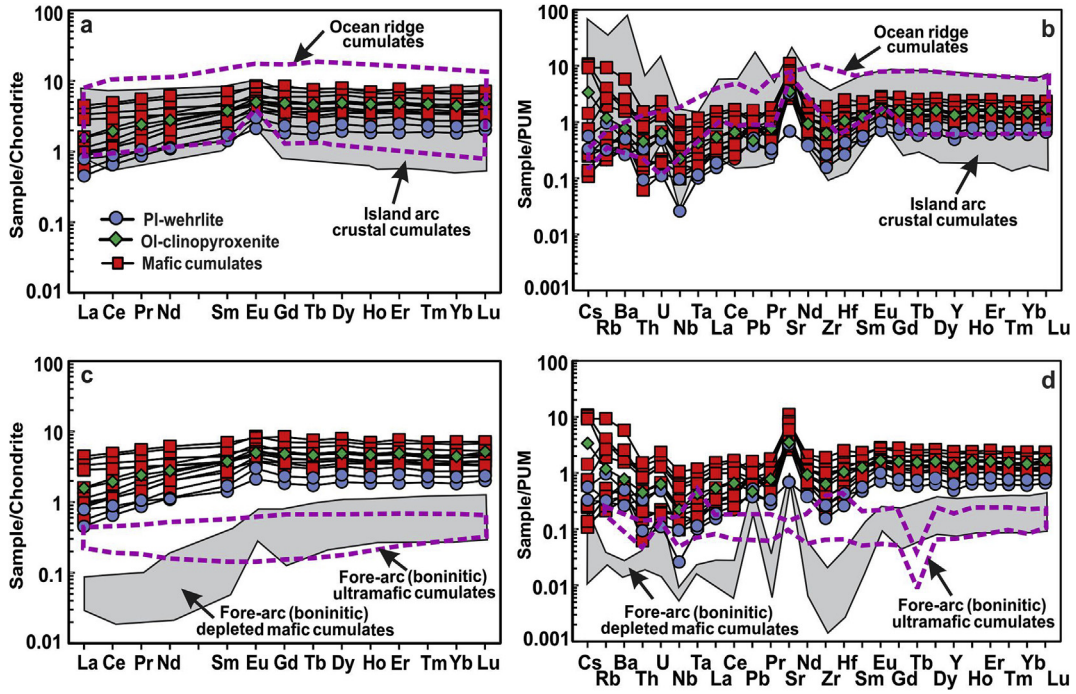

Fig. 10. Chondrite-normalized REE and PUM-normalized trace element patterns of cumulate rocks from the Sabzevar ophiolite compared to (a and b) ocean ridge and island arc crustal cumulates; (c and d) fore-arc (boninitic) ultramafic and depleted mafic crustal cumulates. Data source, ocean ridge cumulates: Ross and Elthon (1997) and Hart et al. (1999); island arc crustal cumulates: Greene et al. (2006); fore-arc (boninitic) ultramafic cumulates: Allahyari et al. (2014); fore-arc depleted mafic crustal cumulates: Marchesi et al. (2009); Normalizing values: Sun and McDonough (1989). PUM: primitive upper mantle.

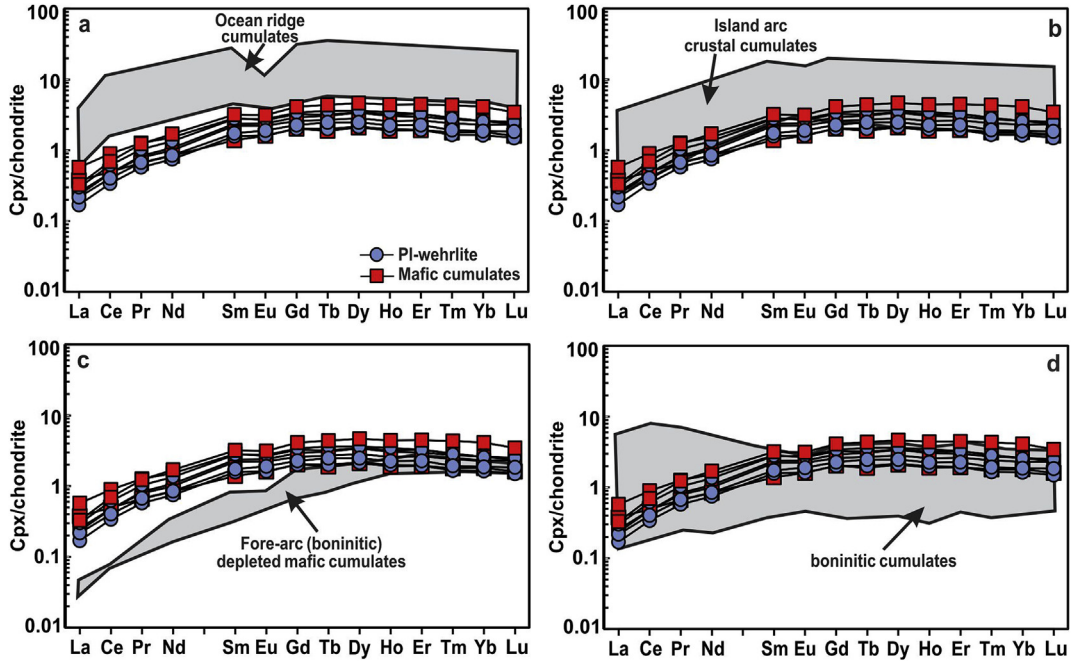

Fig. 11. Chondrite-normalized REE patterns of clinopyroxenes (Cpx) in the cumulate rocks from the Sabzevar ophiolite compared to Cpx composition in (a) ocean ridge cumulates; (b) island arc crustal cumulates; (c) fore-arc (boninitic) depleted mafic cumulates; (d) boninitic cumulates. Data source, ocean ridge cumulate Cpx: Ross and Elthon (1997); island arc crustal cumulate Cpx: Greene et al. (2006); fore-arc depleted mafic cumulate Cpx: Marchesi et al. (2009); boninitic cumulate Cpx: Tribuzio et al. (2008); Normalizing values: Sun and McDonough (1989).

contents) and negligible Eu anomalies (Table 1). The trace element composition of melts in equilibrium with the clinopyroxenes was calculated using the cpx/melt partition coefficients of Ionov et al. (2002) and Tribuzio et al. (2008).

The calculated melts indicate chondrite-normalized REE patterns either slightly depleted or slightly enriched in LREE relative to MREE and HREE [$(La/Sm)_N = 0.74–1.08$ and $(La/Yb)_N = 0.87–1.1$] (Fig. 12). They also show low fractionation of HREE with respect to MREE [$(Sm/Yb)_N = 1.09–1.26$] that is consistent with melting of mantle peridotite in the spinel-facies (e.g., Saccani et al., 2015 and references therein). The REE

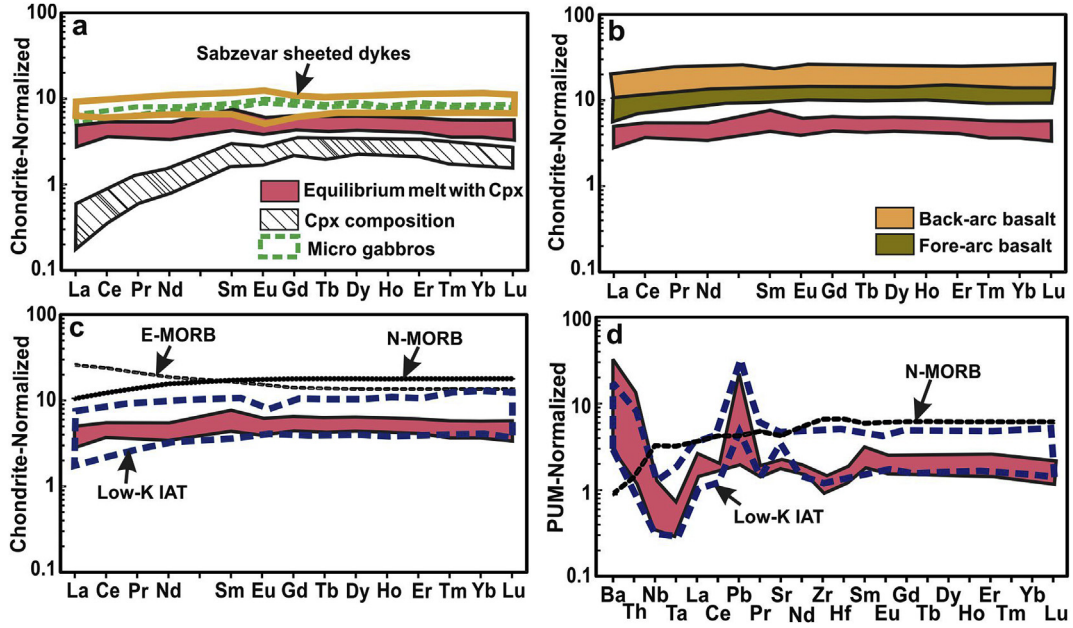

Fig. 12. Chondrite-normalized REE (a–c) and PUM-normalized trace element patterns (d) of calculated melts in equilibrium with clinopyroxenes of cumulate rocks (plagioclase-bearing wehrlite and olivine gabbronorite) from the Sabzevar ophiolite compared to composition of micro grabbroic dike samples within cumulate sequence of the Sabzevar ophiolite, Sabzevar sheeted dikes, clinopyroxenes in the plagioclase-bearing wehrlite and olivine gabbronorite and basaltic magmas from different tectonic settings. Data source, Partition coefficients: Ionov et al. (2002) and Tribuzio et al. (2008); fore-arc and back-arc basalts: Nicholson et al. (2000); low-K IAT basalts: Pearce et al. (1995); Sabzevar sheeted dikes: Rezaei et al. (2018); Normalizing values, N-MORB and E-MORB: Sun and McDonough (1989). PUM: primitive upper mantle.

composition of the calculated melts has been compared to the REE composition of Sabzervar sheeted dikes and the micro grabbroic dike samples within Sabzevar cumulate sequence (samples g-1 and g-18; Supplementary Table 1) (Fig. 12a), fore-arc and back-arc basalts (Nicholson et al., 2000) (Fig. 12b), N-MORB and E-MORB (Sun and McDonough, 1989), and low-K IAT basalts (Pearce et al., 1995) (Fig. 12c). The results indicate that chondrite-normalized REE pattern of the computed melts is parallel to but lower in abundance than that of the micro grabbroic dike samples, as well as Sabzervar sheeted dikes, and coincides with the compositions of low-K IAT basalts. The calculated melts have REE contents clearly lower than those of the MORBs.

The equilibrium melts exhibit high positive Th, Pb and Ba and negative Nb, Ta and Zr anomalies in the PUM-normalized diagram and are enriched in LILE, Pb and LREE but depleted in HFSE such as Nb, Zr and Ta relative to HREE (Fig. 12d). The PUM-normalized trace element patterns of the calculated melts overlap with those of low-K IAT basalts and are different from N-MORB. They are enriched in Ba, Th and Pb, and depleted in HFSEs and REEs with respect to N-MORB (Fig. 12d). These features indicate that parental melt of Sabzevar cumulate rocks was derived from partial melting of a metasomatized mantle source previously depleted by at least one episode of basaltic melt extraction.

The above characteristics strongly suggest that cumulate rocks from the Sabzevar ophiolite were generated by crystal accumulation from a hydrous depleted basaltic/tholeiitic magma, corresponding to IAT-type magmas. This is consistent with mineral chemistry data from the previous study (Rahmani et al., 2017) and the published data geochemistry of co-genetic sheeted dikes and some of basaltic units, which also indicate an IAT affinity (Noghreyan, 1982; Shojaat et al., 2003; Khalatbari Jafari et al., 2013a; Shafaii Moghadam et al., 2014; Rezaei et al., 2018).

7.3. Petrogenesis and tectonic setting

The first phase that crystallizes after olivine in a cumulate sequence is defined by the degree of partial melting that occurred in the mantle source (Jacques and Green, 1980), as well as crystallization pressure and water content. Olivine → plagioclase (plagioclase-type cumulate) is consistent with low, olivine → clinopyroxene (clinopyroxene-type cumulate) is consistent with medium and olivine → orthopyroxene (orthopyroxene-type cumulate) is consistent with high degrees of partial melting. Moreover, Ishiwatari (1985) displayed that the TiO_2 content of clinopyroxene varies in these three types of cumulates. Plagioclase-type cumulates are characterized by high TiO_2 (0.6–0.8 wt.%), clinopyroxene-type cumulates by moderate TiO_2 (0.4 wt.%) and orthopyroxene-type cumulates by low TiO_2 (0.1 wt.%) of clinopyroxene. The crystallization order and the TiO_2 contents of clinopyroxenes (0.14–0.52 wt.%; Rahmani et al., 2017) from cumulate rocks of the Sabzevar ophiolite are correspond to a parental magma being produced by a moderate to high degree of partial melting, leaving a mantle residue represented by the harzburgite (e.g. Jacques and Green, 1980).

In SSZ environments, various types of basaltic magmas can be generated, which indicate a geochemical evolution through time and/or space (Saccani, 2015). They generally begin with MORB-type magma and evolve to boninitic, IAT and calc-alkaline magmas. IAT magmas are typically generated in intra-oceanic island arc environments by partial melting of depleted mantle sources that have experienced metasomatic enrichment through addition of subduction-derived components. Therefore, they show depletion in HFSEs and REEs compared to PUM and variable enrichments in LILEs relative to HFSEs, MREEs and HREEs (De Hoog et al., 2011; Saccani, 2015 and references therein). The low concentrations of HFS elements in subduction zone magmas can be result of: (1) high degree of partial melting of the mantle source (Saccani, 2015 and references therein), (2) stability of minor residual phases (e.g., rutile, zircon and titanite) in the mantle source (Dixon and Batiza, 1979; Pearce, 1996; Wallin and Metcalf, 1998), and (3) remelting of an already depleted mantle source (Green, 1973; Duncan and Green, 1980; Hébert and Laurent, 1990; Koepke et al., 2009).

The LREE depletion relative to HREE, as well as low HFSE contents along with very low content of Ti in the studied clinopyroxenes indicate the origin of Sabzevar cumulate rocks from a depleted source. Moreover, crystallization order and the presence of primary amphibole in the studied rocks indicate crystallization from hydrous magmas. Such magmas are particularly generated in the intra-oceanic subduction zones,

predominantly in island arcs, where hydrous mantle melting was facilitated by the addition of volatiles from the subducting slab (Koepke and Seidel, 2004; Kocak et al., 2005).

In general, two distinct components from the subducted slab have been recognized in island arc magmas, including: (1) a melt generated from the subducted sediments and (2) a fluid flux originated from the dehydration of the down-going oceanic crust (Hochstaedter et al., 2001; Elliott, 2003; Ikeda et al., 2016). The most important component of this fluid is water including seawater released from sediments and altered oceanic crust during compaction process and released water from dehydration of hydrous minerals (Kelley et al., 2003; Saffer and Tobin, 2011). A number of experimental studies have indicated that aqueous solutions are only enriched with water-soluble trace elements such as LILE, Pb and U, while hydrous melts can be enriched with all fluid-mobile trace elements, including LREE, LILE, Pb, U and Th (Zheng and Hermann, 2014). In general, the addition of sediment-derived hydrous melts to the mantle wedge increases LREE, LILE, Th, U and Pb enrichmen and has a considerable role in transporting the water-insoluble elements from subducting slab to the mantle wedge (Elliott et al., 1997; Plank and Langmuir, 1998). Trace elements ratios such as Th/Nb and Ba/Th are little affected by different degrees of partial melting and fractional crystallization, and are commonly used to determine the contributions of subduction-derived components to the mantle source. Ba is highly mobile in slab-derived fluids, therefore it is used as an index of fluid contribution, while Th is used as an index of sediment-drived melt contribution because it is mobile in the melt and enriched in subducted sediments (Brenan et al., 1995; Johnson and Plank, 1999).

In order to determine of subduction components contribution to the mantle source of Sabzevar cumulate rocks, the Ba/Th ratios are plotted vs. Th/Nb ratios (Fig. 13). This plot shows that the magma source of these rocks was influenced by adding both aqueous fluid and sediment-drived melt.

Pirnia et al. (2020) suggested that arc-related rocks of the Nain ophiolite were formed in a geotectonic setting similar to equivalents in the Sabzevar ophiolite. Therefore, to constrain the petrological processes during the genesis of parental melt of the studied cumulate rocks, we used the diagram of semi-quantitative modelling of REE from Pirnia et al. (2020) to provide some constraints on the petrogenesis of basaltic melts in subduction-related settings (Fig. 14). This model has been presented for Nain sheeted dikes, which have IAT affinity and REE compositions comparable with those in Sabzevar sheeted dikes and the calculated melts in equilibrium with clinopyroxenes from Sabzevar cumulate rocks. In this model, the REE composition of the possible mantle source has been computed by adding 0.1% aqueous fluid component and 0.2% melt component of derived from subducted slab to the depleted lherzolite A19 from the Othrys ophiolite in Greece. Lherzolite A19 is a residual mantle after ~20% MORB-type melt extraction and doesn't show traceable enrichment from subducted slab components (Saccani et al., 2017). In Fig. 14, the REE patterns of calculated melts in equilibrium with clinopyroxenes from Sabzevar cumulate rocks are compared to curves calculated for non-modal fractional melting of the computed theoretical mantle source in the spinel lherzolite facies according to source and melting olivine:orthopyroxene:clinopyroxene:spinel modal proportions 0.65:0.28:0.06:0.08 and 0.1:0.64:0.25:0.02, respectively (Kostopoulos and Murton, 1992) and partition coefficients of REE from McKenzie and O'Nions (1991). This diagram indicates that the REE composition of the calculated melts in equilibrium with clinopyroxenes is consistent with ~15% partial melting of the calculated theoretical mantle source in the spinel stability field.

The geochemical and petrological evidences presented in this study indicate that cumulate rocks from the Sabzevar ophiolite were formed in an arc tectonic setting by crystal accumulation from a primary IAT melt, which was originated from depleted mantle sources that underwent metasomatisms by the subduction-related components prior to melting. It is consistent with previous studies on the crustal section of the Sabzevar ophiolite (Noghreyan, 1982; Shojaat et al., 2003; Khalatbari Jafari et al., 2013a, 2013b; Shafaii Moghadam et al., 2014; Rahmani et al., 2017), which suggested intra-oceanic subduction was responsible for producing the SSZ related magmas within the Sabzevar oceanic lithosphere, followed by initiation nucleation and growth of a mature arc. The arc signature of the plutonic crustal rocks of the Sabzevar ophiolite, as well as the occurrence of a well-developed crustal section consist of high-pressure cumulate rocks, gabbroic rocks, sheeted dikes and basaltic units with IAT to calc-alkaline affinities (Shafaii Moghadam et al., 2014, and references therein; Rahmani et al., 2017), which was generated over a considerable period of time (~20 Ma; section 1; Shafaii Moghadam et al., 2014) and intruded by post-ophiolite arc-related felcic stocks and dikes (Shafaii Moghadama et al., 2016) suggest that the Sabzevar ophiolite is similar to volcanic arc-type ophiolite of Dilek and Furnes (2011).

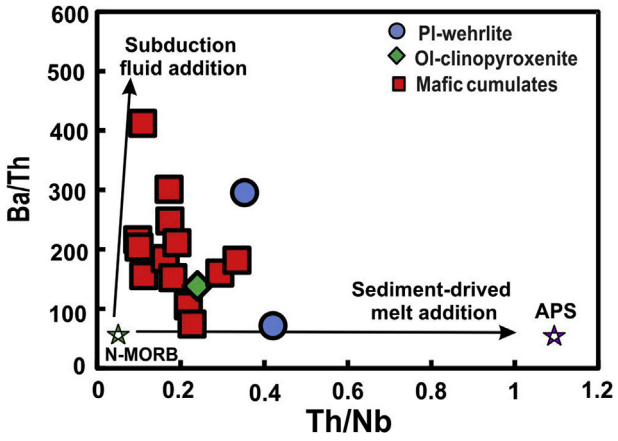

Fig. 13. Ba/Th vs. Th/Nb diagram for cumulate rocks from the Sabzevar ophiolite. Data source, average pelitic sediments (APS): Taylor and McLennan (1985); N-MORB: Sun and McDonough (1989).

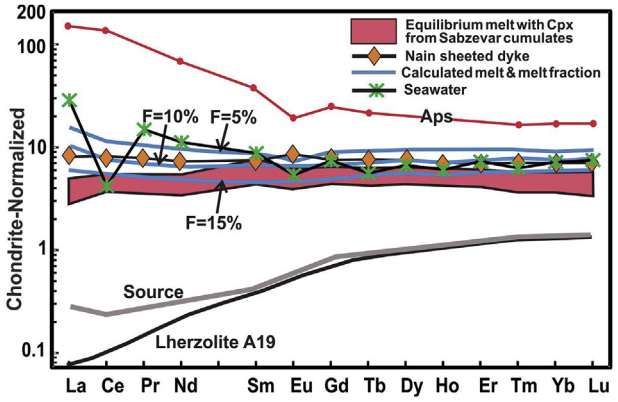

Fig. 14. Chondrite-normalized REE patterns of calculated melts in equilibrium with clinopyroxenes from Sabzevar cumulate rocks compared to calculated parental melts derived from theoretical mantle source by semi-quantitative modelling of REE from Pirnia et al. (2020). The REE values of seawater have been multiplied by 10^6. Data source, average pelitic sediments (APS): Taylor and McLennan (1985); seawater: Deng et al. (2017); Nain sheeted dike: Pirnia et al. (2020); lherzolite A19: Saccani et al. (2017); Source and melting olivine:orthopyroxene:clinopyroxene:spinel modal proportions in the spinel stability field 0.65:0.28:0.06:0.08 and 0.1:0.64:0.25:0.02, respectively (Kostopoulos and Murton, 1992); Normalizing values: Sun and McDonough (1989). Labels indicate partial melting degrees.

8. Conclusions

The petrological and geochemical study of mafic and ultramafic cumulate rocks from eastern part of the Sabzevar ophiolite yields the

following conclusions:

(1) The mafic and ultramafic cumulate rocks comprise plagioclase-bearing wehrlite, olivine clinopyroxenite, olivine gabbronorite, gabbronorite, amphibole gabbronorite and quartz gabbronorite. Based on the petrographic observations, the crystallization order within the cumulate rocks of the Sabzevar ophiolite is olivine ± chromian spinel → clinopyroxene → plagioclase → orthopyroxene → amphibole, correspond to the crystallization order observed in a low Ti and hydrous tholeiitic melt.
(2) The crystallization order and whole-rock major and trace element chemistry, as well as the trace element composition of clinopyroxenes and the calculated equilibrium melts indicate these rocks were produced from an island arc tholeiitic (IAT) magma.
(3) The primary melt of Sabzevar cumulate rocks (hydrous and low Ti, REE and HFSE melt) was generated by a moderate to high degree of partial melting a depleted mantle source, which partially underwent metasomatic enrichment from subduction-derived components prior to melting.
(4) Geochemical and petrological features of the mafic and ultramafic cumulate rocks together with the previous tectonic reconstruction of this region suggest the Sabzevar ophiolite has been formed in an intra-oceanic arc setting.

Declaration of competing interest

The authors declare that they have no known competing financial interests or personal relationships that could have appeared to influence the work reported in this paper.

Acknowledgements

The authors thank the University of Isfahan (Isfahan, Iran) and the Instituto Andaluz de Ciencias de la Tierra (IACT, Granada, Spain) for their support in field work and sample preparation and for providing geochemical analyses facilities. We are grateful to Prof. Kristoffer Szilas, Prof. Tomo Morishita and two anonymous reviewers for their useful and constructive comments that improved the manuscript.

Appendix A. Supplementary data

Supplementary data to this article can be found online at https://doi.org/10.1016/j.gsf.2020.02.004.

References

Allahyari, K., Saccani, E., Rahimzadeh, B., Zeda, O., 2014. Mineral chemistry and petrology of highly magnesian ultramafic cumulates from the Sarve-Abad (Sawlava) ophiolites (Kurdistan, NW Iran): new evidence for boninitic magmatism in intra-oceanic fore-arc setting in the Neo-Tethys between Arabia and Iran. J. Asian Earth Sci. 79, 312–328.
Arvin, M., Robinson, P.T., 1994. The petrogenesis and tectonic setting of lavas from the Baft ophiolitic mélange, southwest of Kerman, Iran. Can. J. Earth Sci. 31, 824–834.
Babazadeh, S.A., De Wever, P., 2004. Early Cretaceous radiolarian assemblages from radiolarites in the Sistan Suture (eastern Iran). Geodiversitas 26, 185–206.
Ballantyne, P., 1992. Petrology and geochemistry of the plutonic rocks of the Halmahera ophiolite, eastern Indonesia, an analogue of modern oceanic forearcs. In: Parson, L.M., Murton, B.J., Browning, P. (Eds.), Ophiolites and Their Modern Oceanic Analogues, vol. 60. Geol. Soc. Lond. Spec. Publ., pp. 179–202
Baroz, R., Macaudiere, J., Montigny, R., Noghreyan, M., Ohnenstetter, M., Rocci, G., 1983. Ophiolites and related formations in the central part of the Sabzevar range (Iran) and possible geotectonic reconstructions. Geodyn. Proj. (Geotraverse) Iran Rep. 51, 519.
Bau, M., 1996. Controls on the fractionation of isovalent trace elements in magmatic an aqueous systems: evidence from Y/Ho, Zr/Hf and lanthanide tetrad effect. Contrib. Mineral. Petrol. 123, 323–333.
Beard, J.S., 1986. Characteristic mineralogy of arc-related cumulate gabbros: implications for the tectonic setting of gabbroic plutons and for andesite genesis. Geology 14, 848–851.
Beccaluva, L., Ohnenstetter, D., Ohnenstetter, M., 1979. Geochemical discrimination between ocean-floor and island-arc tholeiites-application to some ophiolites. Can. J. Earth Sci. 16, 1874–1882.
Beccaluva, L., Di Girolamo, P., Macciotta, G., Morra, V., 1983. Magma affinities and fractionation trends in ophiolites. Ofioliti 8, 307–324.
Beccaluva, L., Serri, G., 1988. Boninitic and low-Ti subduction-related lavas from intra-oceanic arc-backarc systems and low-Ti ophiolites: a reappraisal of their petrogenesis and original tectonic setting. Tectonophysics 146, 291–315.
Beccaluva, L., Macciotta, G., Piccardo, G.B., Zeda, O., 1989. Clinopyroxene compositions of ophiolite basalts as petrogenetic indicator. Chem. Geol. 77, 165–182.
Berberian, M., King, G.C., 1981. Towards a paleogeography and tectonic evolution of Iran. Can. J. Earth Sci. 18, 210–265.
Berger, S., Cochrane, D., Simons, K., Savov, I., Ryan, J.G., Peterson, V.L., 2001. Insights from rare earth elements into the genesis of the Buck Creek complex, Clay County, NC. SE. Geol. 40 (3), 201–212.
Berndt, J., Koepke, J., Holtz, F., 2005. An experimental investigation of the influence of water and oxygen fugacity on differentiation of MORB at 200 MPa. J. Petrol. 46, 135–167.
Borghini, G., Rampone, E., 2007. Postcumulus processes in oceanic-type olivine-rich cumulates: the role of trapped melt crystallization versus melt/rock interaction. Contrib. Mineral. Petrol. 154, 619–633.
Borisenko, L.F., 1967. Trace elements in pyroxenes and amphiboles from ultramafic rocks of the Urals. Mineral. Mag. 36, 403–410.
Brenan, J.M., Shaw, H.F., Ryerson, F.J., Phinney, D.L., 1995. Mineral aqueous fluid partitioning of trace elements at 900 °C and 2.0 GPa: constraints on the trace element chemistry of mantle and deep crustal fluids. Geochem. Cosmochim. Acta 59, 3331–3350.
Brocker, M., Fotoohi rad, G., Burgess, R., Theunissen, S., Paderin, I., Rodionov, N., Salimi, Z., 2013. New age constraints for the geodynamic evolution of the Sistan Suture Zone, eastern Iran. Lithos 170–171, 17–34.
Camuzcuoğlu, M., Bağc, U., Koepke, J., Wolff, P.E., 2017. Tectonic significance of the cumulate gabbros within Kuluncak ophiolitic suite (Malatya, SE Turkey) inferred from geochemical data. Ofioliti 42 (2), 81–103.
Coleman, R.G., 1977. Ophiolites: Ancient Oceanic Lithosphere. Springer, Berlin, p. 229.
Deng, Y., Yuan, F., Zhou, T., Xu, C., Zhang, D., Guo, X., 2015. Geochemical characteristics and tectonic setting of the Tuerkubantao mafic-ultramafic intrusion in West Junggar, Xinjiang, China. Geosci. Front. 6, 141–152.
Debret, B., Andreani, M., Godard, M., Nicollet, C., Schwartz, S., Lafay, R., 2013. Trace element behavior during serpentinization/deserpentinization of an eclogitized oceanic lithosphere: a LA-ICPMS study of the Lanzo ultramafic massif (Western Alps). Chem. Geol. 357, 117–133.
De Hoog, J.C.M., Janak, M., Vrabec, M., Hattori, K.H., 2011. Ultramafic cumulates of oceanic affinity in an intracontinental subduction zone: ultrahigh-pressure garnet peridotites from Pohorje (Eastern Alps, Slovenia). In: Dobrzhinetskaya, L., Faryad, S., Wallis, S., Cuthbert, S. (Eds.), Ultrahigh-Pressure Metamorphism: 25 Years since the Discovery of Coesite. Elsevier Academic Press Inc., New York, pp. 399–439.
Deng, Y., Ren, J., Guo, Q., Cao, J., Wang, H., Liu, C., 2017. Rare earth element geochemistry characteristics of seawater and pore water from deep sea in western Pacific. Nat. Sci. Rep. 7, 16539. https://doi.org/10.1038/s41598-017-16379-1.
Deschamps, F., Guillot, S., Godard, M., Chauvel, C., Andreani, M., Hattori, K., 2010. In situ characterization of serpentinites from fore-arc mantle wedges: timing of serpentinization and behavior of fluid-mobile elements in subduction zones. Chem. Geol. 269, 262–277.
Dey, A., Hussain, M.F., Barman, M.N., 2018. Geochemical characteristics of mafic and ultramafic rocks from the Naga Hills Ophiolite, India: implications for petrogenesis. Geosci. Front. 9, 517–529.
Dilek, Y., 2003. Ophiolite concept and its evolution. In: Dilek, Y., Newcomb, S. (Eds.), Ophiolite Concept and the Evolution of Geological Thought: Boulder, Colorado, vol. 373. Geol. Soc. Am. Bull. Spec. Publ., pp. 1–16
Dilek, Y., Furnes, H., 2011. Ophiolite genesis and global tectonics: geochemical and tectonic fingerprinting of ancient oceanic lithosphere. Geol. Soc. Am. Bull. 123, 387–411.
Dilek, Y., Furnes, H., 2014. Ophiolites and their origins. Elements 10, 93–100. https://doi.org/10.2113/gselements.10.2.93.
Dixon, T.H., Batiza, R., 1979. Petrology and chemistry of recent lavas in the northern Marianas: implications for the origin of island arc basalts. Contrib. Mineral. Petrol. 70, 167–182.
Drouin, M., Godard, M., Ildefonse, B., Bruguier, O., Garrido, C.J., 2009. Geochemical and petrographic evidence for magmatic impregnation in the oceanic lithosphere at Atlantis Massif, Mid-Atlantic Ridge (IODP Hole U1309D, 30° N). Chem. Geol. 264, 71–88.
Dulski, P., 2001. Reference materials for geochemical studies: new analytical data by ICP-MS and critical discussion of reference values. Geostand. Newsl.: J. Geostand. Geoanal. 25, 87–125.
Duncan, R.A., Green, D.H., 1980. Role of multi-stage melting in the formation of oceanic crust. Geology 8, 22–26.
Elliott, T., Plank, T., Zindler, A., White, W., Bourdon, B., 1997. Element transport from slab to volcanic front at the Mariana arc. J. Geophys. Res. 102, 14991–15019.
Elliott, T., 2003. Tracers of the slab. In: Eiler, J. (Ed.), Inside the Subduction Factory, vol. 138. Geophysical Monograph Series AGU, Washington DC, pp. 23–45.
Elthon, D., Casey, J.F., Komor, S., 1982. Mineral chemistry of ultramafic cumulates from the North Arm Mountain massif of the Bay of Islands ophiolite: evidence of high pressure crystal fractionation of oceanic basalts. J. Geophys. Res. 87, 8717–8734.

Elthon, D., 1987. Petrology of gabbroic rocks from the mid-Cayman rise spreading center. J. Geophys. Res. 92, 658–682.
Falloon, T.J., Danyushevsky, L.V., 2000. Melting of refractory mantle at 1.5, 2 and 2.5 Gpa under anydrous and H_2O-undersaturated conditions: implication for the petrogenesis of high-Ca boninites and the influence of subduction components on mantle melting. J. Petrol. 41, 257–283.
Feig, S.T., Koepke, J., Snow, J.E., 2006. Effect of water on tholeiitic basalt phase equilibria: an experimental study under oxidizing conditions. Contrib. Mineral. Petrol. 152, 611–638.
Flanagan, J.F., 1984. Three USGS mafic rock reference samples: W-2, DNC-1, and BIR-1. U. S. Geol. Surv. Bull. 1623, 54.
France, L., Ildefonse, B., Koepke, J., 2013. Hydrous magmatism triggered by assimilation of hydrothermally altered rocks in fossil oceanic crust (Northern Oman ophiolite). G-cubed 14, 2598–2614. https://doi.org/10.1002/ggge.20137.
Gaetani, G.A., Grove, T.L., Bryan, W.B., 1993. The influence of the water on the petrogenesis of subduction-related igneous rocks. Nature 365, 332–334.
Gahlan, H.G., Arai, S., Abu El-Ela, F.F., Tamura, A., 2012. Origin of wehrlite cumulates in the Moho transition zone of the Neoproterozoic Ras Salatit ophiolite, Central Eastern Desert, Egypt: crustal wehrlites with typical mantle characteristics. Contrib. Mineral. Petrol. 163, 225–241.
Garrido, C.J., Bodinier, J.L., Alard, O., 2000. Incompatible trace element partitioning and residence in anhydrous spinel peridotites and websterites from the Ronda orogenic peridotite. Earth Planet Sci. Lett. 181, 341–358.
Gass, I.G., 1989. Magmatic processes at and near constructive plate margins as deduced from the Troodos (Cyprus) and Semail Nappe (N Oman) ophiolites. Geol. Soc. Lond. Spec. Publ. 42, 1–15.
Govindaraju, K., 1994. Compilation of working values and sample description for 383 geostandards. Geostand. Newsl. XVIII (Special Issue), 1–158.
Green, D.H., 1973. Experimental melting studies on a model upper mantle composition at high pressure under water-saturated and water-undersaturated conditions. Earth Planet Sci. Lett. 19 (1), 37–53.
Greene, A.R., DeBari, S.M., Kelemen, P.B., Blusztajn, J., Clift, P.D., 2006. A detailed geochemical study of island arc crust: the Talkeetna Arc section, south-central Alaska. J. Petrol. 47, 1051–1093.
Grove, T.L., Baker, M.B., 1984. Phase equilibrium controls on the tholeiitic versus calc-alkaline differentiation trends. J. Geophys. Res. 89, 3253–3274.
Hart, S.R., Blusztajn, J., Dick, H.J.B., Meyer, P.S., Muehlenbachs, K., 1999. The fingerprint of seawater circulation in a 500-meter section of ocean crust gabbros. Geochem. Cosmochim. Acta 63, 4059–4080.
Hassanipak, A.A., Ghazi, A.M., 1999. Petrology, geochemistry and tectonic setting of the Khoy ophiolite, Northwest Iran. J. Asian Earth Sci. 18, 43–55.
Hawthorne, F.C., Oberti, R., Harlow, G.E., Maresch, W.V., Martin, R.F., Schumacher, J.C., Welch, D., 2012. IMA Report Nomenclature of the amphibole supergroup. Am. Mineral. 97, 2031–2048.
Hébert, R., Laurent, R., 1990. Mineral chemistry of the plutonic section of the Troodos Ophiolite: new constraints for genesis of arc-related ophiolites. In: Malpas, J., Morres, E.M., Panayiotou, A., Xenophontos, C. (Eds.), Ophiolites: Oceanic Crustal Analogues: Proceedings of the Symposium "Troodos 1987". Geological Survey Department of Nicosia, Cyprus.
Hochstaedter, A., Gill, J., Peters, R., Broughton, P., Holden, P., Taylor, B., 2001. Across-arc geochemical trends in the Izu-Bonin arc: contributions from the subducting slab. G-cubed 2. https://doi.org/10.1029/2000GC000105.
Ikeda, Y., Nagao, K., Ishii, T., Matsumoto, D., Stern, R.J., Kagami, H., Arima, M., Bloomer, S.H., 2016. Contributions of slab fluid and sediment melt components to magmatism in the Mariana Arc-Trough system: evidence from geochemical compositions and Sr, Nd, and noble gas isotope systematics. Isl. Arc 25, 253–273.
Ionov, D.A., Bodinier, J.L., Mukasa, S.B., Zanetti, A., 2002. Mechanisms and sources of mantle metasomatism: major and trace element conditions of peridotite xenoliths from Spitzbergen in the context of numerical modelling. J. Petrol. 43 (12), 2219–2259.
Ionov, D.A., Savoyant, L., Dupuy, C., 1992. Application of the ICP-MS technique to trace element analysis of peridotites and their minerals. Geostandards Newsletter 16, 311–315.
Irvine, T.N., Baragar, W.R.A., 1971. A guide to the classification of the common volcanic rocks. Can. J. Earth Sci. 8 (5), 235–458.
Ishiwatari, A., 1985. Alpine ophiolites: product of low- degree mantle melting in a Mesozoic transcurrent rift zone. Earth Planet Sci. Lett. 76, 93–108.
Jacques, A.L., Green, D.H., 1980. Anhydrous melting of peridotite at 0-15 kb pressure and the genesis of tholeiitic basalts. Contrib. Mineral. Petrol. 73, 287–310.
Jagoutz, O., Müntener, O., Burg, J.P., Ulmer, P., Jagoutz, E., 2006. Lower continental crust formation through focused flow in km-scale melt conduits: the zoned ultramafic bodies of the Chilas Complex in the Kohistan arc (NW Pakistan). Earth Planet Sci. Lett. 320, 320–342.
Jiang, S.Y., 2000. Controls on the mobility of high field strength elements (HFSE), U, and Th in an ancient submarine hydrothermal system of the Proterozoic Sullivan Pb-Zn-Ag deposit, British Columbia, Canada. Geochem. J. 34, 341–348.
Jiang, N., Sun, S., Chu, X., Mizuta, T., Ishiyama, D., 2003. Mobilization and enrichment of high-field strength elements during late- and post-magmatic processes in the Shuiquangou syenitic complex, Northern China. Chem. Geol. 200, 117–128.
Johnson, M.C., Plank, T., 1999. Dehydration and melting experiments constrain the fate of subducted sediments. G-cubed 1, 1999GC000014.
Karakaya, N., 2009. REE and HFS element behaviour in the alteration facies of the Erenler Dağı Volcanics (Konya, Turkey) and kaolinite occurrence. J. Geochem. Explor. 101, 185–208.
Kelemen, P.B., Koga, K., Shimizu, N., 1997. Geochemistry of gabbro sills in the crust-mantle transition zone of the Oman ophiolite: implications for the origin of the oceanic lower crust. Earth Planet Sci. Lett. 146 (3–4), 475–488.
Kelemen, P.B., Hanghøj, K., Greene, A.R., 2003. One view of the geochemistry of subduction-related magamatic arcs, with emphasis on primitive andesite and lower crust. In: Rudnick, R.L., Holland, H.D., Turekian, K.K. (Eds.), Treatise on Geochemistry 3. Elsevier–Pergamon, pp. 593–659.
Kelley, K.A., Plank, T., Ludden, J., Staudigel, H., 2003. Composition of altered oceanic crust at ODP Sites 801 and 1149. G-cubed 4, 1–21.
Khalatbari Jafari, M., Babaie, H.A., Gani, M., 2013b. Geochemical evidence for Late Cretaceous marginal arc-to-back-arc transition in the Sabzevar ophiolitic extrusive sequence, northeast Iran. J. Asian Earth Sci. 70 (71), 209–230.
Khalatbari Jafari, M., Babaie, H.A., Mirzaie, M., 2013a. Geology, petrology and tectonomagmatic evolution of the plutonic crustal rocks of the Sabzevar ophiolite, northeast Iran. Geol. Mag. 150 (5), 862–884.
Kocak, K., Isik, F., Arslan, M., Zedef, V., 2005. Petrological and source region characteristics of ophiolitic hornblende gabbros from the Aksarav and Kavseri regions, central Anatolian crystalline complex, Turkey. J. Asian Earth Sci. 25, 883–891.
Koepke, J., Seidel, E., 2004. Hornblendites within ophiolites of Crete, Greece: evidence for amphibole-rich cumulates derived from an iron-rich tholeiitic melt. Ofioliti 29, 159–175.
Koepke, J., Feig, S.T., Snow, J., Freise, M., 2004. Petrogenesis of oceanic plagiogranites by partial melting of gabbros: an experimental study. Contrib. Mineral. Petrol. 146, 414–432.
Koepke, J., Schoenborn, S., Oelze, M., Wittmann, H., Feig, S.T., Hellebrand, E., Boudier, F., Schoenberg, R., 2009. Petrogenesis of crustal wehrlites in the Oman ophiolite: experiments and natural rocks. G-cubed 10 (10), Q10002. https://doi.org/10.1029/2009GC002488.
Kostopoulos, D.K., Murton, B.J., 1992. Origin and distribution of components in boninite genesis: significance of the OIB component. In: Parson, L.M., Murton, B.J., Browning, P. (Eds.), Ophiolites and Their Modern Oceanic Analogues, vol. 60. Geol. Soc. Lond. Spec. Publ., pp. 133–154
Lensch, G., 1980. Major element geochemistry of the ophiolites in north–eastern Iran. In: Panayotou, A. (Ed.), Ophiolites, Proceedings International Ophiolite Symposium, Cyprus 1979. Geological Survey Department, Cyprus, pp. 398–401.
Lensch, G., Davoudzadeh, M., 1982. Ophiolites in Iran. Neues Jahrbuch für Geologie und Paläontologie-Monatshefte 5, 306–320.
Lindenberg, H.G., Görler, K., Jacobshagen, V., Ibbeken, H., 1984. Post–Paleozoic stratigraphy, structure and orogenic evolution of the southern Sabzevar zone and the Taknar block (Khorassan, NE Iran). Neues Jahrbuch Geol. Palaontol. Abhand. 168, 287–326.
Liu, C.Z., Zhang, C., Yang, L.Y., Zhang, L.L., Ji, W.Q., Wu, F.Y., 2014. Formation of gabbronorites in the Purang ophiolite (SW Tibet) through melting of hydrothermally altered mantle along a detachment fault. Lithos 205, 127–141.
Marchesi, C., Garrido, C.J., Godard, M., Proenza, J.A., Gervilla, F., Blanco-Moreno, J., 2006. Petrogenesis of highly depleted peridotites and gabbroic rocks from Mayarí-Baracoa ophiolite belt (Eastern Cuba). Contrib. Mineral. Petrol. 151, 717–736.
Marchesi, C., Garrido, C.J., Godard, M., Belley, F., Ferré, E., 2009. Migration and accumulation of ultra-depleted subduction-related melts in the Massif du Sud ophiolite (New Caledonia). Chem. Geol. 266, 171–186.
Mattei, M., Cifelli, F., Muttoni, G., Zanchi, A., Berra, F., Mossavvari, F., Eshraghi, S.A., 2012. Neogene block-rotation in Central Iran: evidence from paleomagnetic data. Geol. Soc. Am. Bull. 124, 943–956. https://doi.org/10.1130/B30479.1.
Mattei, M., Cifelli, F., Muttoni, G., Rashid, H., 2014. Post-Cimmerian (Jurassice-Cenozoic) paleogeography and vertical axis tectonic rotations of Central Iran and the Alborz Mountains. J. Asian Earth Sci. 102, 92–101. https://doi.org/10.1016/j.jseaes.2014.09.038.
McKenzie, D., O'Nions, R.K., 1991. Partial melt distributions from inversion of rare earth element concentrations. J. Petrol. 32, 1021–1091.
Metcalf, R.V., Shervais, J.W., 2008. Suprasubduction-zone ophiolites: is there really an ophiolite conundrum?. In: Wright, J.E., Shervais, J.W. (Eds.), Ophiolites, Arcs and Batholiths: A Tribute to Cliff Hopson, vol. 438. Geological Society of America, Special Papers, pp. 191–222.
Meyer, P.S., Henry, J.B., Dick, H.J.B., Geoffrey Thompson, G., 1989. Cumulate gabbros from the Southwest Indian Ridge, 54° S-7°16' E: implications for magmatic processes at a slow spreading ridge. Contrib. Mineral. Petrol. 103, 44–63.
Miyashiro, A., 1973. The Troodos ophiolitic complex was probably formed in an island arc. Earth Planet Sci. Lett. 19, 218–224.
Miyashiro, A., 1975. Classification characteristics and origin of ophiolites. J. Geol. 83, 249–281.
Muravyeva, N.S., Belyatsky, B.V., Senin, V.G., Ivanov, A.V., 2014. Sr-Nd-Pb isotope systematics and clinopyroxene-host disequilibrium in ultra-potassic magmas from Toro-Ankole and Virunga, East-African Rift: implications for magma mixing and source heterogeneity. Lithos 210, 260–277.
Nicholson, K.N., Black, P.M., Picard, C., 2000. Geochemistry and tectonic significance of the Tangihua ophiolite complex, New Zealand. Tectonophysics 321, 1–15.
Niu, Y., Gilmore, T., Mackie, S., Greig, A., Bach, W., 2002. Mineral chemistry, whole-rock compositions, and petrogenesis of Leg 176 gabbros. In: Natland, J.H., Dick, H.J.B., Miller, D.J., Von Herzen, R.P. (Eds.), Proceedings of the Ocean Drilling Program. Sci. Results, vol. 176, pp. 1–60.
Noghreyan, M., 1982. Evolution geochimique, mineralogique et structurale d'un edifice ophiolitique singulier: le massif de Sabzevar (partie centrale), NE de l'Iran. Ph.D. thesis, Universite de Nancy, France, p. 239 (in French).

Omrani, H., Moazzen, M., Oberhänsli, R., Altenberger, U., Lange, M., 2013. The Sabzevar blueschists of the North–Central Iranian micro–continent as remnants of the Neotethys–related oceanic crust subduction. Int. J. Earth Sci. 102, 1491–1512.
Otamendi, J.E., Tiepolo, M., Walker, B.A., Cristofolini, E.A., Tibaldi, A.M., 2016. Trace elements in minerals from mafic and ultramafic cumulates of the central Sierra de Valle Fértil, Famatinian arc, Argentina. Lithos 240–243, 355–370.
Pál-Molnár, E., Batki, A., Almási, E., Kiss, B., Upton, B.G.J., Markl, G., Odling, N., Harangi, S., 2015. Origin of mafic and ultramafic cumulates from the Ditrău Alkaline Massif, Romania. Lithos 239, 1–18.
Parlak, O., Delaloye, M., Bingol, E., 1996. Mineral chemistry of ultramafic and mafic cumulates as an indicator of the arc-related origin of the Mersin ophiolite (southern Turkey). Geol. Rundsch. 85, 647–661.
Parlak, O., Hock, V., Delaloye, M., 2000. Supra-subduction zone origin of the Pozanti-Karsanti ophiolite (southern Turkey) deduced from whole–rock and mineral chemistry of the gabbroic cumulates. In: Bozkurt, E., Winchester, J.A., Piper, J.D.A. (Eds.), Tectonics and Magmatism in Turkey and the Surrounding Area, vol. 173. Geol. Soc. Lond. Spec. Publ., pp. 219–234
Parlak, O., Hock, V., Delaloye, M., 2002. The supra-subduction zone Pozanti-Karsanti ophiolite, southern Turkey: evidence for high-pressure crystal fractionation of ultramafic cumulates. Lithos 65, 205–224.
Paton, C., Hellstrom, J., Paul, B., Woodhead, J., Hergt, J., 2011. Iolite: freeware for the visualisation and processing of mass spectrometric data. J. Anal. Atomic Spectrom. 26, 2508–2518.
Pearce, J.A., Baker, P.E., Harvey, P.K., Luff, I.W., 1995. Geochemical evidence for subduction fluxes, mantle melting and fractional crystallization beneath the south sandwich island arc. J. Petrol. 36, 1073–1109.
Pearce, J.A., Norry, M.J., 1979. Petrogenetic implications of Ti, Zr, Y, and Nb variations in volcanic rocks. Contrib. Mineral. Petrol. 69, 33–43.
Pearce, J.A., 1996. A user's guide to basalt discrimination diagrams. In: Wyman, D.A. (Ed.), Trace Element Geochemistry of Volcanic Rocks: Applications for Massive Sulphide Exploration, vol. 12. Geological Association of Canada, Short Course Note, pp. 79–113.
Pearce, J.A., 2003. Supra-subduction zone ophiolites: the search for modern analogues. In: Dilek, Y., Newcomb, S. (Eds.), Ophiolite Concept and the Evolution of Geologic Thought, vol. 373. Geological Society of America, Special Paper, pp. 269–294.
Pearce, J.A., 2008. Geochemical fingerprinting of oceanic basalts with applications to ophiolite classification and the search for Archean oceanic crust. Lithos 100, 14–48.
Pirnia, T., Saccani, E., Torabi, G., Chiari, M., Goričan, Š., Barbero, E., 2020. Cretaceous tectonic evolution of the Neo-Tethys in Central Iran: evidence from petrology and age of the Nain-Ashin ophiolitic basalts. Geosci. Front. 11, 57–81. https://doi.org/10.1016/j.gsf.2019.02.008.
Piccardo, G.B., Guarnieri, L., 2011. Gabbro-norite cumulates from strongly depleted MORB melts in the Alpine–Apennine ophiolites. Lithos 124, 200–214.
Plank, T., Langmuir, C.H., 1998. The chemical composition of subducting sediment and its consequences for the crust and mantle. Chem. Geol. 145, 325–394.
Rahmani, F., Noghreyan, M., Mackizadeh, M.A., 2017. Mineral chemistry of the ultramafic and mafic cumulates in the eastern part of the Sabzevar ophiolite (NE Iran): evidence for formation of high pressure cumulates in thickened arc crust. Neues Jahrbuch Geol. Palaontol. Abhand. 286 (3), 303–328.
Rahmani, F., 2018. Petrology and Geochemistry of Peridotites and Gabbros in the Eastern Part of the Sabzevar Ophiolite (NE of Central Iran). Ph.D. thesis, University of Isfahan, Iran, p. 242.
Rezaei, Z., Noghreyan, M., Saccani, E., 2018. Petrology and geochemistry of sheeted dikes and pillow lavas from the Sabzevar ophiolitic melange (northeast Iran): new constraints for the late Cretaceous evolution of the Neotethys oceanic basin between the central Iranian microcontinent and eurasia. Ofioliti 43 (2), 147–172.
Rollinson, H., 1993. Using Geochemical Data; Evaluation, Presentation, Interpretation. Longman Scientific and Technical, Harlow UK, p. 352.
Ross, C.S., Foster, M.D., Myers, A.T., 1954. Origin of dunites and olivine rich inclusions in basaltic rocks. Am. Mineral. 39, 693–737.
Ross, K., Elthon, D., 1997. Cumulus and postcumulus crystallization in the oceanic crust: major and trace element geochemistry of LEG 153 gabbroic rocks. In: Karson, J.A., Cannat, M., Miller, D.J., Elthon, D. (Eds.), Proceedings of the Ocean Drilling Program. Scientific Results, vol. 153, pp. 333–350.
Rossetti, F., Nasrabady, M., Vignaroli, G., Theye, T., Gerdes, A., Razavi, S.M.H., Moin Vaziri, H., 2010. Early Cretaceous migmatitic mafic granulites from the Sabzevar range (NE Iran): implications for the closure of the Mesozoic peri–Tethyan oceans in central Iran. Terra. Nova 22, 26–34.
Rossetti, F., Nasrabady, M., Theye, T., Gerdes, A., Monié, P., Lucci, F., Vignaroli, G., 2014. Adakite differentiation and emplacement in a subduction channel: the late Paleocene Sabzevar magmatism (NE Iran). Geol. Soc. Am. Bull. 126, 317–343.
Saccani, E., Beccaluva, L., Photiades, A., Zeda, O., 2011. Petrogenesis and tectonomagmatic significance of basalts and mantle peridotites from the Albanian–Greek ophiolites and sub-ophiolitic mélanges. New constraints for the Triassic–Jurassic evolution of the Neo-Tethys in the Dinaride sector. Lithos 124, 227–242.
Saccani, E., Dilek, Y., Marroni, M., Pandolfi, L., 2015. Continental margin ophiolites of Neotethys: remnants of ancient ocean-continent transition zone (OCTZ) lithosphere and their geochemistry, mantle sources and melt evolution patterns. Episodes 38, 230–249.
Saccani, E., 2015. A new method of discriminating different types of post-Archean ophiolitic basalts and their tectonic significance using Th-Nb and Ce-Dy-Yb systematics. Geosci. Front. 6, 481–501.
Saccani, E., Dilek, Y., Photiades, A., 2017. Time-progressive mantle-melt evolution and magma production in a Tethyan marginal sea: a case study of the Albanide-Hellenide ophiolites. Lithosphere 10, 35–53. https://doi.org/10.1130/L602.1.
Saffer, D.M., Tobin, H.J., 2011. Hydrogeology and mechanics of subduction zone forearcs: fluid flow and pore pressure. Annu. Rev. Earth Planet Sci. 39, 157–186.
Salvi, S., Fontan, F., Monchoux, P., Williams Jones, A., Eand Moine, B., 2000. Hydrothermal mobilization of high field strength elements in alkaline igneous systems: evidence from the Tamazeght Complex (Morocco). Econ. Geol. 95, 559–576.
Saunders, A.D., Tarney, J., Marsh, N.G., Wood, D.A., 1980. Ophiolites as ocean crust or marginal basin crust: a geochemical approach. In: Panayiotou, A. (Ed.), Ophiolite. Geological Survey Department, Cyprus, pp. 193–204.
Sengör, A.M.C., 1990. A new model for the late Paleozoic- Mesozoic tectonic evolution of Iran and implication for Oman. In: Robertson, A.H.F., Searle, M.P., Ries, A.C. (Eds.), The Geology and Tectonics of the Oman Region, vol. 49. Geol. Soc. Lond. Spec. Publ., pp. 797–831
Serri, G., 1981. The petrochemistry of ophiolite gabbroic complexes. A key for the classification of ophiolites into Low-Ti and High-Ti types. Earth Planet Sci. Lett. 52, 203–212.
Shafaii Moghadam, H., 2009. The Nain-Baft Ophiolites (Central Iran): Age, Structure and Origin. Ph.D. thesis. Shahid Beheshti University, Tehran, Iran, p. 532.
Shafaii Moghadam, H., Zaki Khedr, M., Arai, S., Stern, R.J., Ghorbani, G., Tamura, A., Ottley, C.J., 2013. Arc-related harzburgite–dunite–chromitite complexes in the mantle section of the Sabzevar ophiolite, Iran: a model for formation of podiform chromitites. Gondwana Res. https://doi.org/10.1016/j.gr.2013.09.007.
Shafaii Moghadam, H., Corfu, F., Chiaradia, M., Stern, R.J., Ghorbani, G., 2014. Sabzevar Ophiolite, NE Iran: progress from embryonic oceanic lithosphere into magmatic arc constrained by new isotopic and geochemical data. Lithos 210–211, 224–241.
Shafaii Moghadam, H., Stern, R.J., 2015. Ophiolites of Iran: keys to understanding the tectonic evolution of SW Asia: (II) Mesozoic ophiolites. J. Asian Earth Sci. 100, 31–59.
Shafaii Moghadama, H., Rossetti, F., Lucci, F., Chiaradia, M., Gerdes, A., Lopez Martinez, M., Ghorbani, G., Nasrabady, M., 2016. The calc-alkaline and adakitic volcanism of the Sabzevar structural zone (NE Iran): implications for the Eocene magmatic flare-up in Central Iran. Lithos 248–251, 517–535.
Shervais, J.W., 2001. Birth, death, and resurrection: the life cycle of suprasubduction zone ophiolites. G-cubed 2 (1), 2000GC000080. https://doi.org/10.1029/2000GC000080.
Shervais, J.W., Kimbrough, D.L., Renne, P., Hanan, B.B., Murchey, B., Snow, C.A., Schuman, M.Z., Beaman, B.J., 2004. Multi-stage origin of the coast range ophiolite, California: implications for the life cycle of supra-subduction zone ophiolites. Int. Geol. Rev. 46, 289–315.
Shirdashtzadeh, N., Torabi, G., Meisel, T.C., Arai, S., Bokhari, S.N.H., Samadi, R., Gazel, E., 2014. Origin and evolution of metamorphosed mantle peridotites of Darreh Deh (Nain ophiolite, Central Iran): implications for the Eastern Neo-Tethys evolution. Neues Jahrbuch Geol. Palaontol. Abhand. 273, 89–120.
Shojaat, B., Hassanipak, A.A., Mobasher, K., Ghazi, A.M., 2003. Petrology, geochemistry and tectonics of the Sabzevar ophiolite, North Central Iran. J. Asian Earth Sci. 21, 1053–1067.
Stern, R.J., 2004. Subduction initiation: spontaneous and induced. Earth Planet Sci. Lett. 226, 275–292.
Stöcklin, J., 1974. Possible ancient continental margins in Iran. In: Burk, C.A., Drake, C.L. (Eds.), The Geology of Continental Margins. Springer, New York, pp. 837–887.
Sun, S.S., Nesbitt, R.W., 1978. Geochemical characteristics of mid ocean ridge basalts. Earth Planet Sci. Lett. 44, 119–138.
Sun, S.S., McDonough, W.F., 1989. Chemical and isotopic systematics of oceanic basalts: implications for mantle composition and processes. In: Saunders, A.D., Norry, M.J. (Eds.), Magmatism in the Ocean Basins, vol. 42. Geol. Soc. Lond. Spec. Publ., pp. 313–345
Takin, M., 1972. Iranian geology and continental drift in the Middle East. Nature 235, 147–150.
Tanirli, M., Rizaoglu, T., 2016. Whole-rock and mineral chemistry of mafic cumulates from the Low-Ti ophiolite in the southern part of Kahramanmaras, Turkey. Russ. Geol. Geophys. 57, 1398–1418.
Taylor, S.R., McLennan, S.M., 1985. The Continental Crust: its Composition and Evolution: an Examination of the Geochemical Record Preserved in Sedimentary Rocks. Blackwell Scientific Publication, Oxford, p. 312.
Torabi, G., 2010. Early Oligocene alkaline lamprophyric dikes from the Jandaq area (Isfahan province, Central Iran) evidence of central–east Iranian microcontinent confining oceanic crust subduction. Isl. Arc 19, 277–291.
Torabi, G., 2013. Chromitite absence, presence and chemical variation in ophiolites of Central Iran (Nain, Ashin, Anarak and Jandaq). Neues Jahrbuch für Geologie und Paläontologie-Abhandlungen 267, 171–192.
Torabi, G., Arai, S., Koepke, J., 2011. Metamorphosed mantle peridotites from Central Iran (Jandaq area, Isfahan province). Neues Jahrbuch für Geologie und Paläontologie-Abhandlungen 261, 129–150.
Tribuzio, R., Tiepolo, M., Fiameni, S., 2008. A mafic–ultramafic cumulate sequence derived from boninite-type melts (Niagara Icefalls, northern Victoria Land, Antarctica). Contrib. Mineral. Petrol. 155, 619–633.
Wallin, E.T., Metcalf, R.V., 1998. Supra-subduction zone ophiolite formed in an extensional fore-arc: trinity Terrane, Klamath Mountains, California. J. Geol. 106, 591–608.
Wilson, M., 1989. Igneous Petrogenesis. Unwin Hyman, London, p. 466.
Whitney, D.L., Evans, B.W., 2010. Abbreviations for names of rock-forming minerals. Am. Mineral. 95, 185–187.
Zheng, Y.-F., Hermann, J., 2014. Geochemistry of continental subduction-zone fluids. Earth Planets and Space 66, 93. https://doi.org/10.1186/1880-5981-66-93.